Reprinted from

TECTONOPHYSICS

INTERNATIONAL JOURNAL OF GEOTECTONICS AND THE GEOLOGY AND PHYSICS OF THE INTERIOR OF THE EARTH

Tectonophysics 280 (1997) 83–106

Temperature- and strain-rate-dependent microfabric evolution in monomineralic mylonite: evidence from in situ deformation of norcamphor

Marco Herwegh [a,*], Mark R. Handy [b], Renée Heilbronner [c]

[a] *Geologisches Institut, Baltzerstraße 1, Universität Bern, CH-3012 Bern, Switzerland*
[b] *Institut für Geowissenschaften, Universität Giessen, Giessen, Germany*
[c] *Geologisches Institut und Abteilung für Wissenschaftliche Photographie, Universität Basel, Basel, Switzerland*

Received 27 January 1996; accepted 31 October 1996

ELSEVIER

TECTONOPHYSICS

Scope of the journal

Tectonophysics is an international medium for the publication of original studies and comprehensive reviews in the field of geotectonics and the geology and physics of the earth's crust and interior. The editors will endeavour to maintain a high scientific level and it is hoped that with its international coverage the journal will contribute to the sound development of this field.

(Text continued on inside back cover)

PRINTED IN THE NETHERLANDS

ELSEVIER

Tectonophysics 280 (1997) 83–106

TECTONOPHYSICS

Temperature- and strain-rate-dependent microfabric evolution in monomineralic mylonite: evidence from in situ deformation of norcamphor

Marco Herwegh [a,*], Mark R. Handy [b], Renée Heilbronner [c]

[a] Geologisches Institut, Baltzerstraße 1, Universität Bern, CH-3012 Bern, Switzerland
[b] Institut für Geowissenschaften, Universität Giessen, Giessen, Germany
[c] Geologisches Institut und Abteilung für Wissenschaftliche Photographie, Universität Basel, Basel, Switzerland

Received 27 January 1996; accepted 31 October 1996

Abstract

Norcamphor ($C_7H_{10}O$) was subjected to plane strain simple shear in a see-through deformation rig at four different strain rate and temperature conditions. Two transient stages in the microfabric evolution to steady state are distinguished. The grain scale mechanisms associated with the microstructural and textural evolution vary with the applied temperature, strain rate and strain. In high-temperature–low-strain-rate experiments, computer integrated polarization microscopy reveals that the texture evolution is closely related to the crystallographic rotation paths and rotation rates of individual grains. High *c*-axis rotation rates at low to intermediate shear strains are related to the development of a symmetrical *c*-axis cross girdle by the end of the first transient stage ($\gamma = 1.5$ to 2). During the second transient stage ($\gamma = 1.5$ to 6), the cross girdle yields to an oblique *c*-axis single girdle as *c*-axis rotation rates decrease and the relative activity of grain boundary migration recrystallization increases. Steady state ($\gamma > 8$) is characterized by a stable end orientation of the sample texture and the cyclic growth, rotation and consumption of individual grains within the aggregate.

Keywords: experimental structural geology; rock analogue; microfabric; texture; dynamic recrystallization

1. Introduction

Over the past thirty years, microstructural analysis of experimentally and naturally deformed mylonite have shown that dislocation glide and creep are intimately associated with the development of a crystallographic preferred orientation (CPO), usually termed 'texture' in the materials science literature. Mylonitic texture yields information about both the physical conditions and kinematics of deformation, but the difficulty in distinguishing the effects of temperature, strain-rate and strain on texture remains one of the basic limitations in applying textures to interpret the deformational history of mylonite. It appears that the relative contributions of these effects to texture cannot be discerned without understanding the way in which texture evolves with strain.

Although most workers now agree that texture formation in polycrystalline aggregates involves the rotation of intracrystalline slip systems, there is considerable controversy as to the precise way in which

* Corresponding author. Tel.: +41 (31) 631-8764; fax: +41 (31) 631-4843; e-mail: herwegh@geo.unibe.ch

PII S0040-1951(97)00139-X

these systems rotate. One concept, the so-called 'stable end orientation' concept, envisages the rotation of slip systems into irrotational orientations. Intracrystalline slip occurs parallel to the overall shearing direction within glide planes oriented parallel to the shear zone boundary (e.g., Schmidt, 1927). This idea is supported by complete texture analyses of naturally and experimentally deformed mylonites and assumes that the stable end orientation maximizes the resolved shear stress on the active slip systems (Schmid and Casey, 1986; Schmid et al., 1987; Etchecopar and Vasseur, 1987; Law et al., 1990; Schmid, 1994). Dynamic recrystallization is believed to play a fundamental role in preserving this stable end orientation by eliminating grains that are unfavourably oriented for intracrystalline glide (Schmid and Casey, 1986). A more recent concept, the so-called 'ideal orientation' concept (Wenk and Christie, 1991), relates texture to orientation-dependent rotation rates of the active intracrystalline slip systems. To paraphrase Wenk and Christie (1991), ideal orientations are pole figure maxima corresponding to orientations for which the rotations of slip systems are slowest (p. 1096 in Wenk and Christie, 1991). This rate-dependent rotation of slip systems has been simulated in computer models using both the Taylor–Bishop–Hill (TBH; Lister et al., 1978; Lister and Hobbs, 1980) and viscoplastic self-consistent (VPSC) theories of polycrystalline plasticity (Wenk et al., 1989). In the absence of dynamic recrystallization, however, no stable end orientations can ever be attained in such dynamic systems. The modelling work of Jessell (1988a,b) and Jessell and Lister (1990) shows that modifying TBH theory to account for dynamic recrystallization can produce startlingly realistic model quartz microfabrics.

So far, neither of these concepts has been adequately tested because microfabrics of samples from natural shear zones and from high-pressure experiments record mostly finite strain, precluding a reconstruction of the crystallographic rotation trajectories of individual grains during shearing. An alternative approach adopted below is to conduct experiments on organic analogue materials with a relatively low melting temperature and to monitor their microfabric as it evolves under the optical microscope (Means, 1977, 1989). Although the crystallography of many organic materials is not well known, previous work has shown that the textures and microstructures produced in such materials bear a striking resemblance to those found in naturally deformed rock (e.g., Means, 1989; Herwegh and Handy, 1996).

In the following, we report on a series of experiments conducted on norcamphor which we combined with computer-integrated polarization microscopy (CIP; Panozzo-Heilbronner and Pauli, 1993) to document continuously the evolution of a steady state texture during simple shearing. The experiments were carried out at four different homologous temperature–strain rate conditions:

(1) high homologous temperature–low strain rate experiments (HT–LS);

(2) high homologous temperature–high strain rate experiments (HT–HS; see also Herwegh and Handy, 1996);

(3) intermediate homologous temperature–high strain rate experiments (IT–HS); and

(4) low homologous temperature–high strain rate experiments (LT–HS; see Table 1 for experimental conditions).

The *c*-axis rotation paths and velocities determined in norcamphor with the CIP method suggest that texture evolution in polycrystalline aggregates

Table 1

Experimental conditions: high temperature–low strain rate (HT–LS), high temperature–high strain rate (HT–HS), intermediate temperature–high strain rate (IT–HS) and low temperature–high strain rate (LT–HS)

	HT–LS	HT–HS	IT–HS	LT–HS
T (°C)	25	25	10	4
T_h	0.81	0.81	0.77	0.76
Shear strain rate	4.0×10^{-5}	5.5×10^{-4}	5.5×10^{-4}	5.5×10^{-4}
Maximum attained shear strain (γ)	7.9	10.5	9	5
Experiment duration (h)	55	5.25	4.5	2.5

involves elements of both the stable end orientation and ideal orientation concepts outlined above. We conclude the paper with a list of criteria that should enable geologists to distinguish the effects of strain and temperature in quartz mylonite that has undergone simple shearing.

2. Sample preparation and analytical procedures

We used a Means-Urai rig to deform norcamphor ($C_7H_{10}O$) in plane strain, simple shear (see Jessell, 1986; Means, 1989; fig. 1a in Herwegh and Handy, 1996 for a detailed description of the experimental configuration). Herwegh and Handy (1996) have found many striking similarities between the microfabric of experimentally deformed norcamphor and that of naturally deformed, mylonitic quartz. Norcamphor is uniaxial negative and probably has hexagonal crystallographic symmetry as inferred from hexagonal dendrites formed during sublimation on glass (see fig. 2.5 in Bons, 1993). Unfortunately, the high sublimation rate of norcamphor at room temperature precludes the use of standard X-ray goniometry to identify its crystallography and potential glide systems.

We prepared the sample in the same way as already described in Herwegh and Handy (1996): Norcamphor was mixed with corundum grinding powder prior to cold and hot pressing. In contrast to our previous sample preparation procedure, however, hot pressing of the current sample batch lasted longer (96–172 h) at temperatures ranging from 35° to 45°C. Fig. 1 depicts pole figures for the initial, hot-pressed textures of the samples prior to the simple shearing experiments. Note that coaxial flattening during hot pressing induces *c*-axis point maxima parallel to the *Y* direction in Fig. 1b,c (see HT–LS, IT–HS and LT–HS columns in Fig. 1b,c). The initial texture of the samples in the HT–HS experiments comprises concentric *c*-axis small circle patterns about the principle stress (σ_1) direction for hot pressing (HT–HS column in Fig. 1b,c). In contrast, the initial textures of the other experiments contain *c*-axes maxima along the periphery of the pole figures in Fig. 1b (see also elongate maxima in Fig. 1c). These textures may reflect sample flowage parallel to the frosted grips of the glass slides during flattening in the *Y* direction in Fig. 1a. Note that the incomplete small circle along the periphery of the pole figure in the initial HT–LS texture (Fig. 1b and Fig. 2) reflects an artefact of the measuring method. Because the HT–LS run was the first experiment in which we applied the CIP method (see below), we did not realize that the tilting angle we applied during digital imaging was too low. Consequently, norcamphor *c*-axes with azimuths in the 220–290° range at intermediate to high inclinations were not imaged correctly. Based on later experiments, we surmise that correct measurement of the texture would have yielded a small circle *c*-axis pattern symmetrically disposed about the hot pressing σ_1 direction.

We applied two methods of texture analysis in the analogue experiments:

(1) a modified optical 'Achsenverteilungsanalyse' or AVA (Sander, 1950) involving U-stage measurement of norcamphor *c*-axes whose general orientation within the microstructure was established from the interference colour of grains (for a detailed description of the procedure, see Herwegh and Handy, 1996); and

(2) computer-integrated polarization microscopy (CIP; Panozzo-Heilbronner and Pauli, 1993, 1994).

Using the U-stage has a basic problem: rapid annealing of the samples precludes deforming the sample to higher strains after *c*-axis measurement. Thus, the experiment must be repeated several times, each time to a different shear strain, such that the *c*-axes are measured in a different sample at the end of each run. A quantitative evaluation of the rotation paths of *c*-axes for individual grains can therefore not be obtained with the U-stage. The main advantage of the CIP method (method 2) is that it allows such an evaluation and we have applied it to track *c*-axis trajectories in the new experiments reported below. The CIP software package generates a *c*-axis orientation image from 22 digital infrared images by calculating grey value images representing the azimuths and inclinations of the *c*-axes at each of the pixels of the entire grain aggregate (Panozzo-Heilbronner and Pauli, 1993, 1994). Eighteen of the twenty-two images are taken at 10° rotation intervals and four images in tilted orientations (see configuration in Herwegh, 1996). The *c*-axis orientations are assigned characteristic colours (see colours and their reference code in Figs. 2–4). The *c*-axis orientations are then plotted in a standard *c*-axis pole figure using

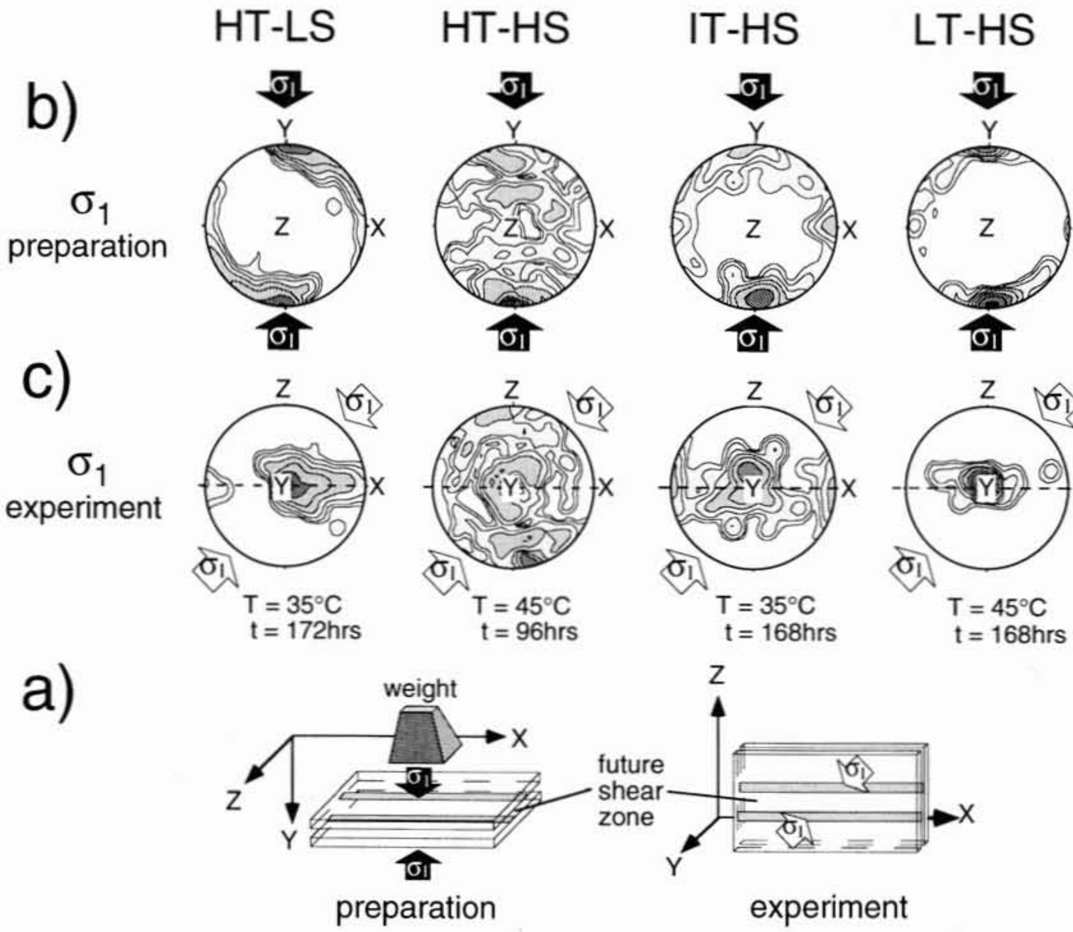

Fig. 1. Equal-area projections of initial textures after hot pressing during sample preparation. (a) Flattening plane is oriented east–west in the pole figures, perpendicular to the σ_1 direction of hot pressing (black arrows). (b) Simple shear plane is oriented east–west in the pole figures, corresponding to the SZB at 45° to the σ_1 direction during the experiments (white arrows). Note that the initial textures in the first and second rows are identical; a 90° clockwise rotation about the X sample preparation axis transforms the pole figures in (a) to those shown in (b). (c) Specimen axes during sample preparation and simple shearing experiments. T = hot pressing temperature, t = hot pressing duration.

the program 'Stereoplot XL' (Mancktelow, 1993). Table 2 shows the methods employed and the frequency of textural analysis performed during each of the experiments. In the HT–LS experiments, the strain rate was sufficiently low (4×10^{-5} s^{-1}) to obtain seventeen orientation images without interrupting the experiments. In contrast, all high strain rate experiments had to be interrupted for 10 to 15 min in order to record the 22 digital images required for each orientation image. To minimize sample annealing during these intermissions, the number of orientation images per increment of shear strain was reduced (see IT–HS and LT–HS columns in Table 2). The resulting decrease in temporal resolution was compensated for by taking additional digital images every 5 min without interrupting the experiment. The public domain software NIH image 1.57 (Rasband, 1995) allowed us to animate these images and to calculate changes in the areas of individual grains and grain aggregates with strain (e.g., Fig. 5).

3. Microfabric evolution

Our previous work with norcamphor has shown that microfabric changes involve the simultaneous activity of several interactive mechanisms from the

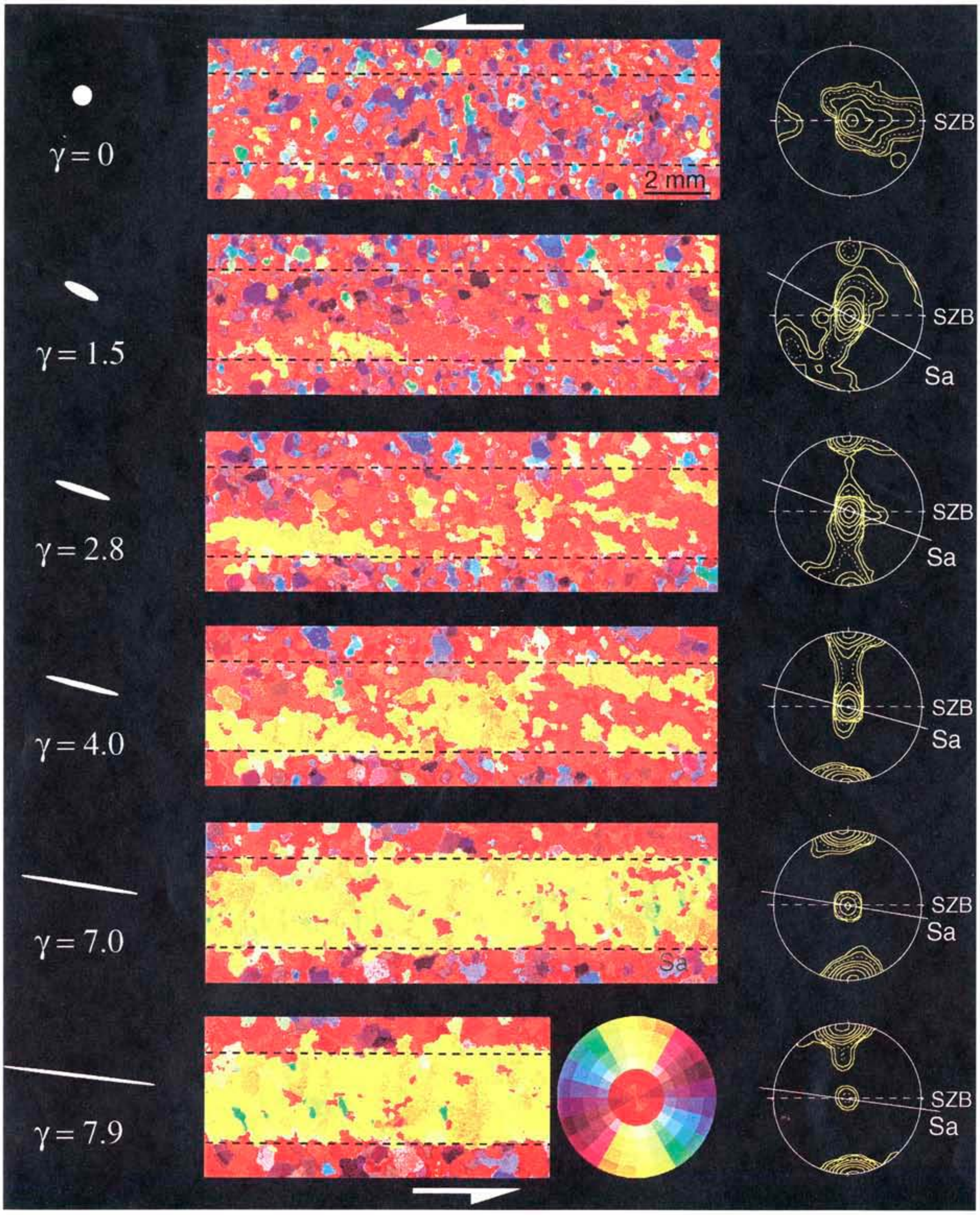

Fig. 2. HT–LS microfabric evolution. Finite strain ellipses (first column) CIP-generated orientation images (second column) and colour reference pole figure (bottom of second column), contoured c-axis pole figures (third column). Shear zone boundary (dashed horizontal lines) and long axis of the finite strain ellipse (line labelled *Sa*). Contour intervals of the pole figures are 0.25, 0.5, 1.0 (dashed), 2, 4, 8, 16, 32 times uniform distribution.

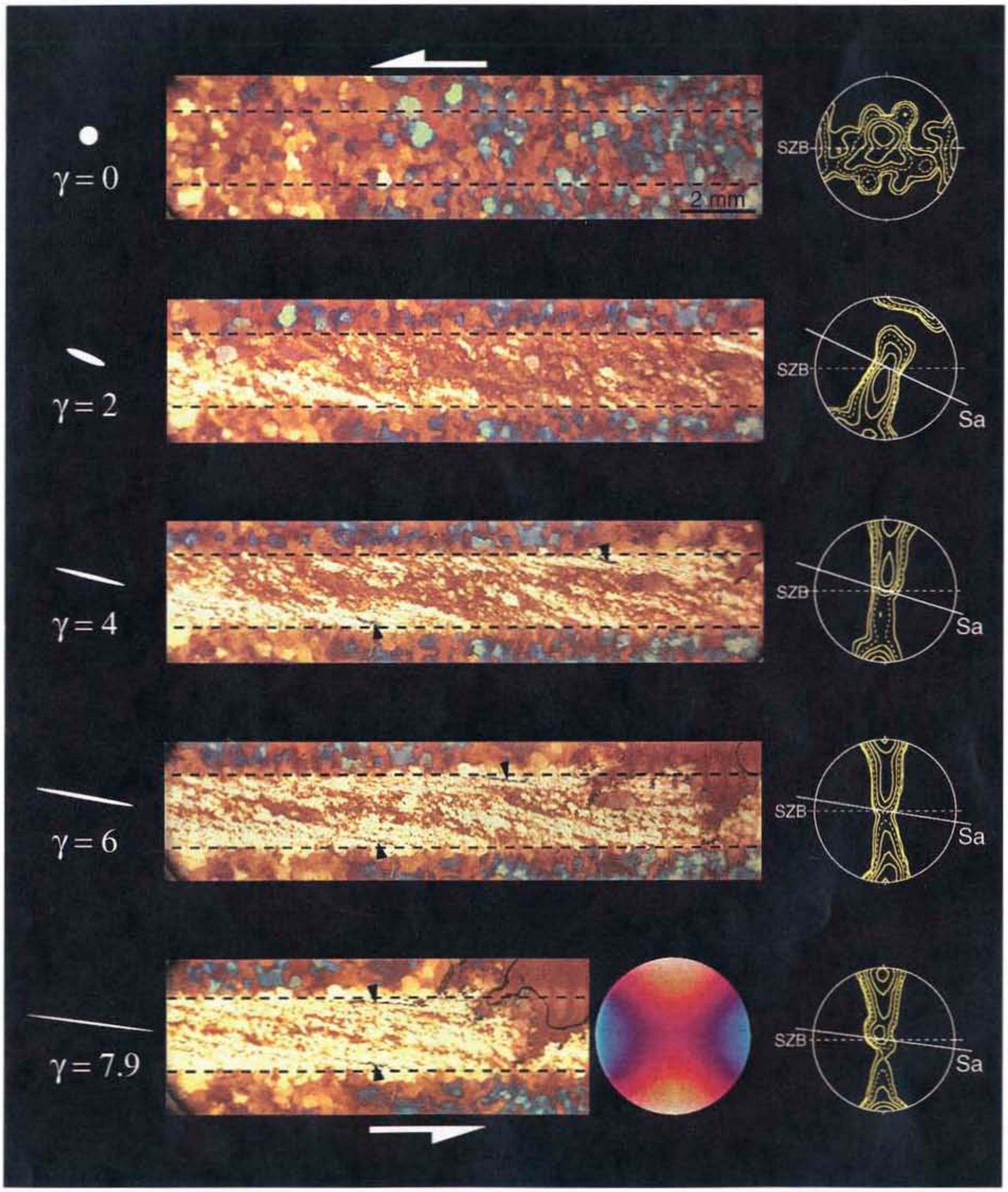

Fig. 3. IT–HS microfabric evolution. Finite strain ellipses (first column), optical photographs of microfabric (second column) and colour reference pole figure (bottom of second column), contoured c-axis pole figures (third column). Note that, the reference colour pole figure (= conoscopic image) corresponds to a set up where the analyzer, polarizer and compensator are rotated 45° counterclockwise from their standard position. Cracks (blacks arrows), shear zone boundary (dashed horizontal lines) and long axis of the finite strain ellipse (line labelled *Sa*) are indicated in the pole figures. Contour intervals of the pole figures are 0.25, 0.5, 1.0 (dashed), 2, 4, 8, 16, 32 times uniform distribution.

sub- to the supragranular scale (Herwegh and Handy, 1996). We applied the concept of a mechanism assemblage to describe the simultaneous activity of such mechanisms, with the term 'mechanism' used in a rather broad sense to refer to any grain scale process that involves changes in microfabric. Our new work below indicates that textural and microstructural changes leading to a steady state microfabric are strongly dependent on temperature and strain rate. The recognition of different relative activities of mechanisms with strain allowed us to discern two transient stages in the microfabric evolution. Although the nature and duration of these stages varied with temperature and strain rate, both stages were discerned in all of the experiments described below.

3.1. High temperature–low strain rate (HT–LS) experiments

3.1.1. First transient stage

At $\gamma = 0$ to 1.5, glide-induced vorticity ('shear-induced component of vorticity' of Lister, 1982; Lister and Williams, 1983) is manifest by the glide-induced rotation and elongation of individual grains. This results in an oblique shape preferred orientation (SPO) at 60° to the SZB. Strain-dependent changes in the CIP-generated colours of grains reflect changes in grains' *c*-axis orientations (Fig. 2). These orientations can be read from the colour-coded pole figure at the bottom of Fig. 2. The glide-induced rotation of the *c*-axes as well as the simultaneous growth of yellow and magenta grains via grain boundary migration leads to the rapid consumption of grains that are unfavourably oriented for intracrystalline glide parallel to the SZB (e.g., appearance of favourably oriented yellow grains and disappearance of unfavourably oriented blue and purple grains in Figs. 2 and 5a). The average grain size increases (Figs. 6 and 7) and a weak domainal microfabric develops at the end of the first transient stage. At somewhat higher shear strains ($\gamma = 1.5$), the texture consists of a *c*-axis cross girdle that is symmetrically disposed with respect to the long axis of the finite strain ellipse (see third column in Fig. 2). The concentration of *c*-axes in the centre of the pole figure is partly inherited from the initial texture (Fig. 1b,c) but also reflects incipient rotation of some *c*-axes into an orientation consistent with prism glide parallel to the SZB (see discussion section below). The *c*-axes point maxima of the cross girdle at the periphery of the pole figure in Fig. 2 were generated with the mechanism assemblage described above.

3.1.2. Second transient stage

Between $\gamma = 1.5$ and $\gamma = 6$, intense grain boundary migration recrystallization combined with the coalescence of yellow grains (Means and Dong, 1982; see fig. 9 in Herwegh and Handy, 1996) strengthens the domainal character of the microfabric until the microfabric only consists of yellow and magenta grains (Fig. 2). The average grain area increases linearly with strain, reflecting the high activity of grain boundary migration (Figs. 6 and 7). The same phenomenon was observed in one of the octachloropropane experiments of Jessell (1986, fig. 7, run TO-63). Progressive subgrain rotation recrystallization ('rotational recrystallization' of Poirier and Guillope, 1979) is especially active in yellow grains and contributes to the complete dynamic recrystallization of the entire microfabric at shear strains above 2.8. Interestingly, the average grain SPO already becomes strain invariant at shear strains of 1.5. This is consistent with observations of SPO in octachloropropane (Ree, 1991) and norcamphor deformed at higher strain rates (Herwegh and Handy, 1996). The progressive strengthening of the domainal microfabric is closely related to the consumption of magenta grains by yellow grains (see Fig. 5a) and involves a textural transition from a symmetrical *c*-axis cross girdle to a *c*-axis single girdle. The latter is oriented subperpendicular to the SZB but obliquely oriented with respect to the main foliation (see second and third columns of Fig. 2).

3.1.3. Steady state

At shear strains above 6, both the texture and the relative area of yellow and magenta grains become strain invariant, indicating the attainment of textural and microstructural steady state (Fig. 2). Although microfabric appears to be strain invariant on the sample scale, the continuous activity of high- and low-angle grain boundary migration and subgrain rotation recrystallization replenishes the microfabric with a steady supply of new, presumably less-strained grains (see below). The details of this renewal process are quite complex: when

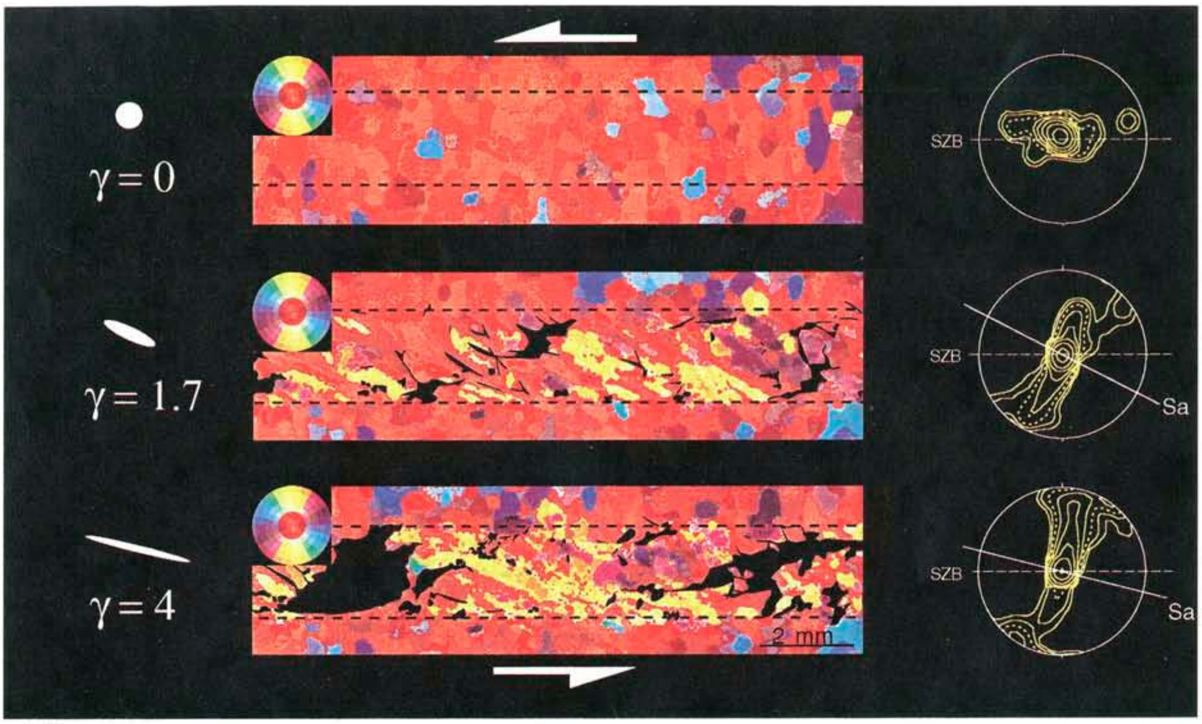
γ = 0
γ = 1.7
γ = 4
SZB
Sa
2 mm

Fig.4

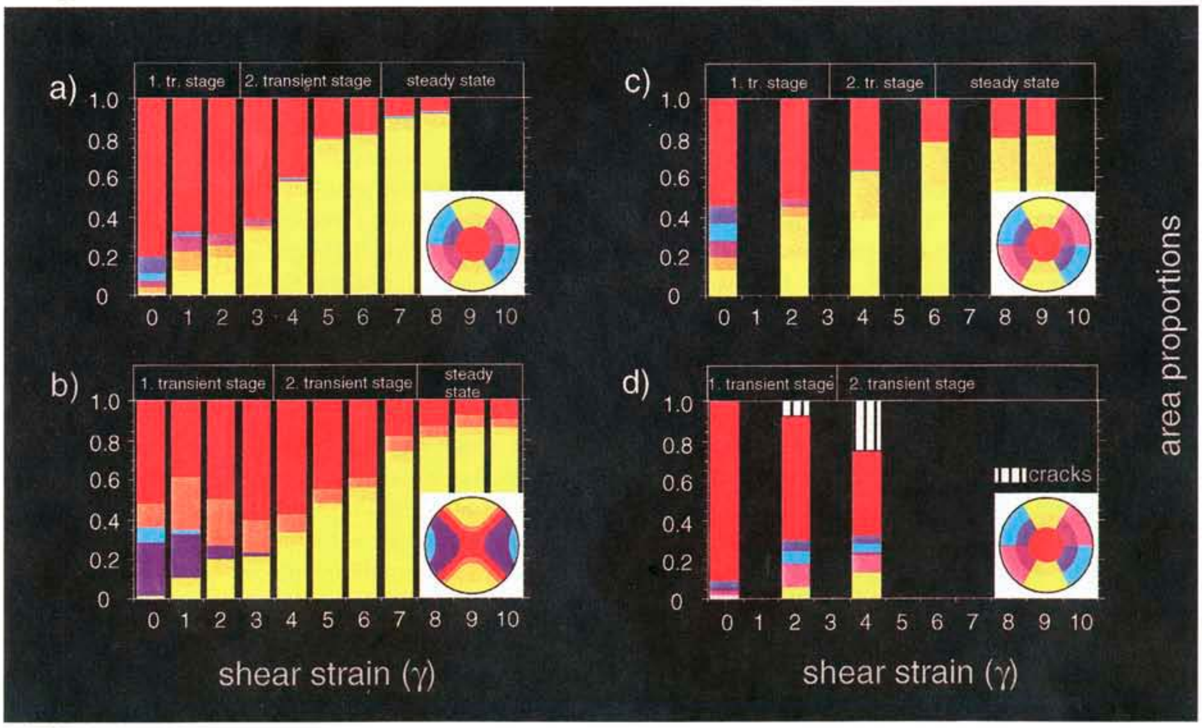
a)
1. tr. stage
2. transient stage
steady state
b)
1. transient stage
2. transient stage
steady state
c)
1. tr. stage
2. tr. stage
steady state
d)
1. transient stage
2. transient stage
cracks
area proportions
shear strain (γ)

Fig.5

Table 2

Chart showing the methods used to document the microstructural and textural evolution during the experiments: digital infrared pictures, normal 35 mm photographs, CIP (computer-integrated polarization microscopy), U–St. (U-stage measurement of *c*-axes)

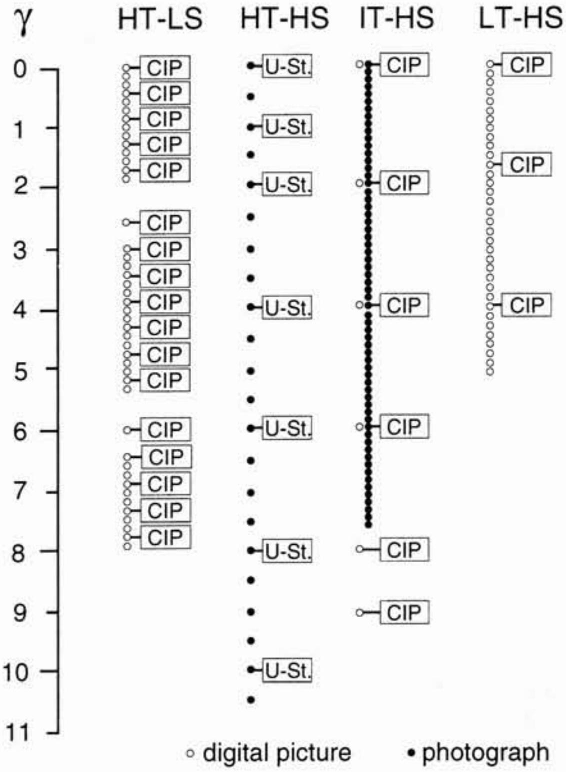

The evolution of the microstructure in all experiments was also documented with videotape (HT–HS) or computer animation of the digital images (HT–LS, IT–HS, LT–HS).

observing the grain boundaries of yellow and magenta grains, we were surprised to find that old magenta grains are never completely consumed by the yellow grains. Instead, they undergo cycles of shrinkage and growth. Burg et al. (1986) observed similar oscillatory growth and consumption of grains in polycrystalline ice undergoing simple shear. The oscillatory behaviour of magenta and yellow grains preserves a stable proportion of differently coloured and oriented grains within the sample (Fig. 5a). A statistically constant proportion of differently oriented grains on the sample scale is also manifest in the texture which comprises two stable *c*-axis point maxima, one parallel to the *Y* specimen axis and the other slightly oblique to the SZB normal (see bottom two rows of Fig. 2). Note that Figs. 6 and 7 seem to indicate that grain size increases continuously with strain and therefore has not reached steady state. Unfortunately, the weak colour contrasts between similarly oriented grains at high shear strains pre-

Fig. 4. LT–HS microfabric evolution. Finite strain ellipses (first column) CIP-generated *c*-axis orientation images (second column) and colour reference pole figure (top left-hand corner of each orientation image), contoured *c*-axis pole figures (third column). Shear zone boundary (dashed horizontal lines) and long axis of the finite strain ellipse (line labelled *Sa*). Contour intervals of the pole figures are 0.25, 0.5, 1.0 (dashed), 2, 4, 8, 16, 32 times uniform distribution.

Fig. 5. Relative areal proportions of grains with a specific crystallographic orientation as a function of increasing shear strain for HT–LS (a), HT–HS (b), IT–HS (c) and LT–HS (d) experiments. Corresponding CIP-generated colour reference pole figures are shown.

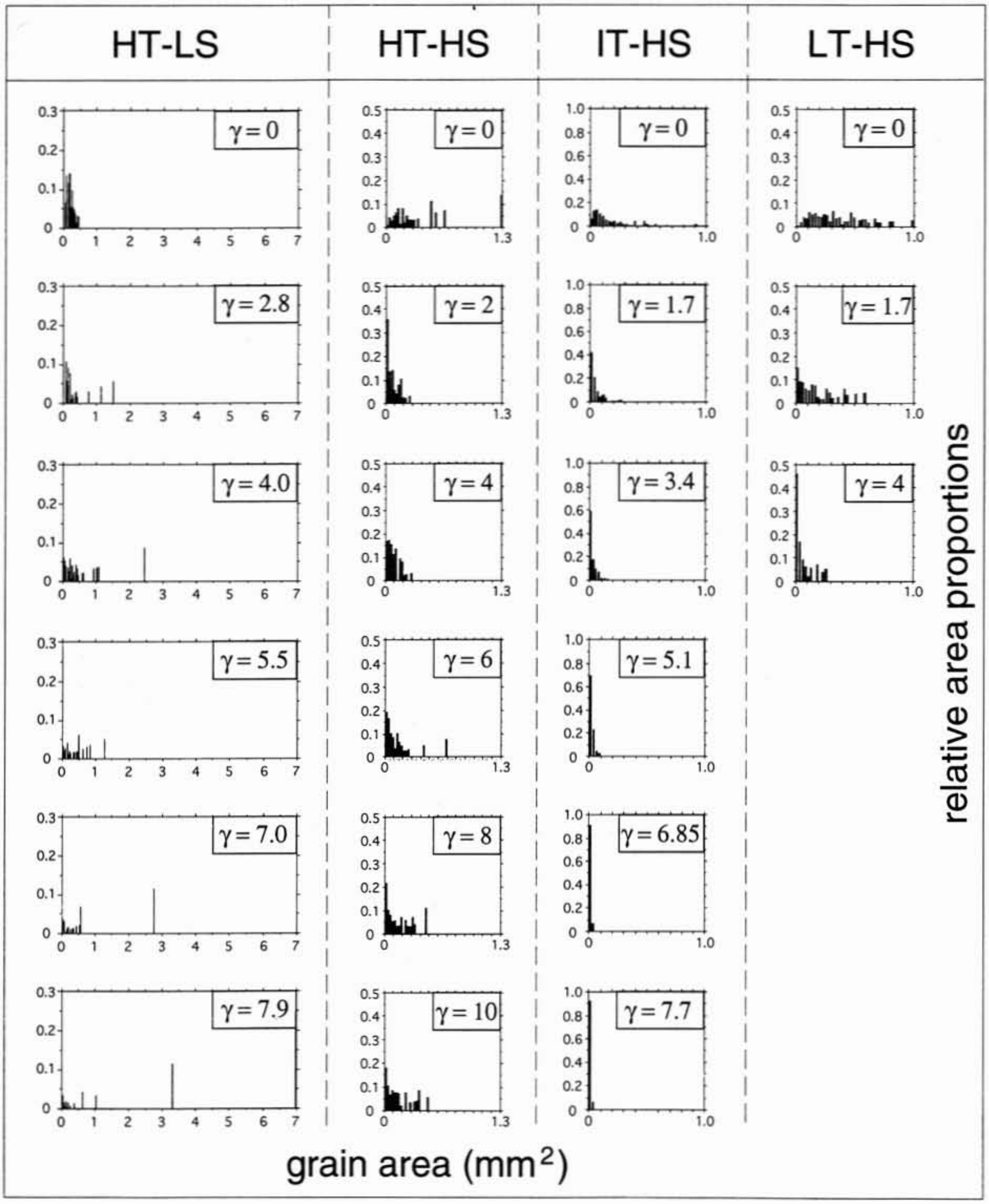

Fig. 6. Evolution of grain area distribution with shear strain in the experiments. The grain area evolution depends on temperature and strain rate (see text for explanation). Note that the scaling on the horizontal grain area axis and the vertical area proportion axis vary in the different columns.

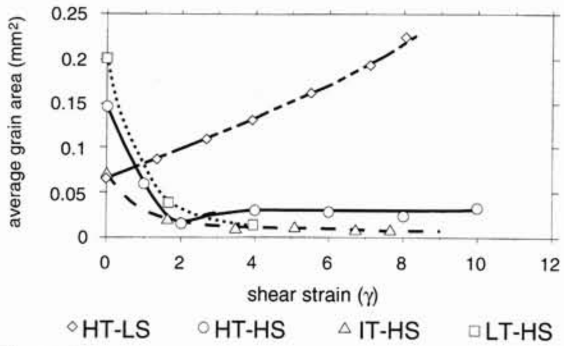

Fig. 7. Change in grain area with shear strain for the different experimental conditions (see text for explanation).

clude the accurate measurement of grain shape and size, so that the estimates for the HT–LS runs at $\gamma \geq 6$ in Figs. 6 and 7 may not accurately reflect the true grain size.

The HT–LS microstructures described here are very similar to the HT–HS microstructures reported in Herwegh and Handy (1996), indicating that strain rate has a relatively modest effect on microfabric evolution at high homologous temperature (compare Fig. 2 of this paper with fig. 2 of Herwegh and Handy, 1996). Nevertheless, there are some differences between the HT–HS and HT–LS microfabrics that can be related to varied strain rate. During the first transient stage in the evolution of the HT–HS microfabrics, subgrain rotation recrystallization and rigid body rotation are the predominant mechanisms (Fig. 8a), whereas grain boundary migration is less active than in the HT–LS experiments (Fig. 8a). This is associated with a significant decrease in grain size (Figs. 6 and 7) as well as with the development of a c-axis cross girdle at relatively higher

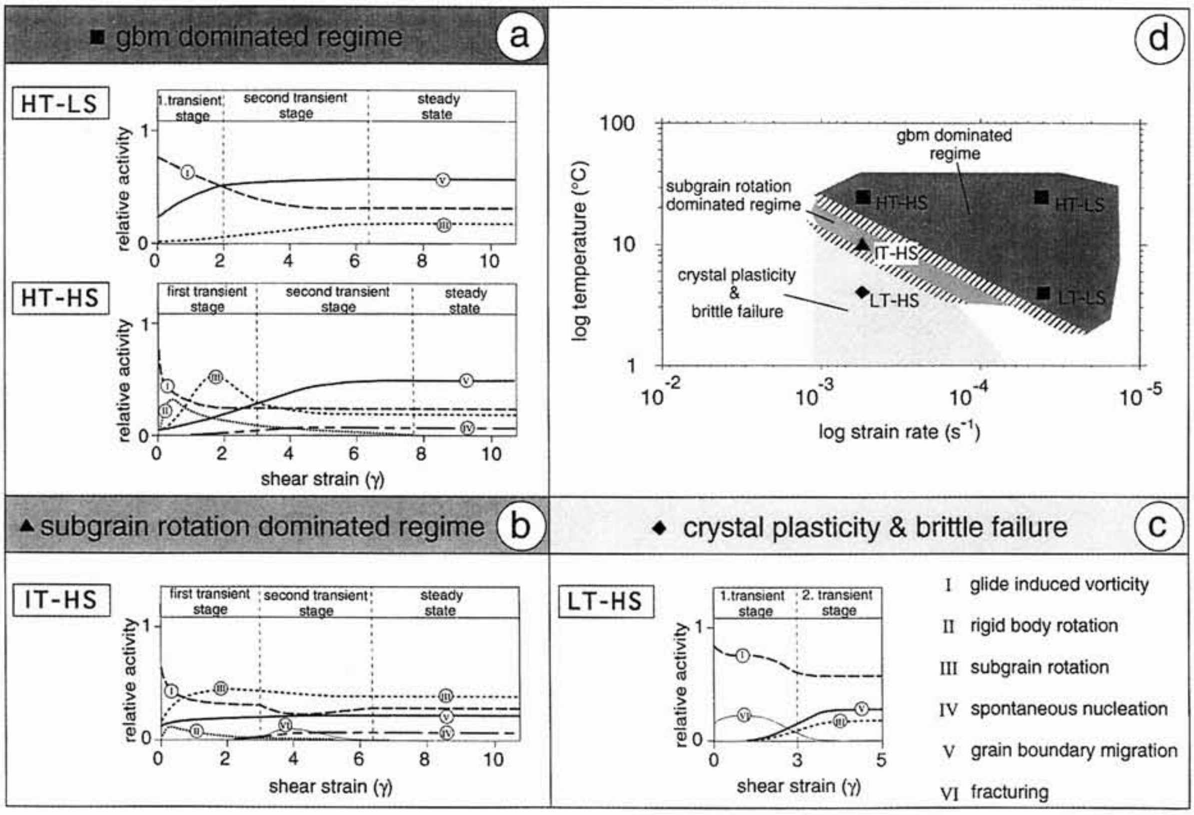

Fig. 8. Schematic diagrams showing the variation in mechanism assemblage as a function of shear strain for the different experiments: (a) HT–LS and HT–HS, (b) IT–HS, (c) LT–HS. (d) Temperature vs. strain rate plot of the dominant grain scale mechanisms in experimental deformation of norcamphor (see text for explanation). Note the LT–LSR (low temperature–low strain rate) experiments are not reported in this work but they yield the same microfabrics as the HT–HS experiments.

shear strains ($\gamma = 2$) in the HT–HS experiments. In the second transient stage, the width of the domains in the HT–HS microfabric is narrower than that of the HT–LS microfabrics (370 μm vs. 570 μm). At steady state, both experiment types have a similar mechanism assemblage (Fig. 8a). In case of the HT–HS experiments, however, grain boundary mobility is lower and spontaneous nucleation of new grains is an additional mechanism associated with the conservation of a strain invariant microfabric (Fig. 8a). Spontaneous nucleation is discussed below in greater detail.

As already demonstrated in Herwegh and Handy (1996), the high-temperature norcamphor microfabrics are very similar to those of naturally quartz mylonite deformed under upper greenschist to amphibolite facies conditions (compare fig. 12 of Herwegh and Handy, 1996 with Fig. 2 of this work). In both norcamphor and quartz samples, the microstructure comprises an oblique SPO and relatively large grains with bulged grain boundaries. These features reflect the strong component of grain boundary migration in simple shear. In norcamphor, we observed that small equi-axed grains originate by progressive subgrain rotation. We infer a similar origin for such grains in quartz. Nevertheless, differences in the positions of c-axis point maxima between quartz and norcamphor textures probably reflect differences in the relative activity of slip systems (compare fig. 12 of Herwegh and Handy, 1996 with Fig. 2 of this work).

3.2. Intermediate temperature–high strain rate (IT–HS) experiments

3.2.1. First transient stage

The mechanism assemblage for the first transient stage ($\gamma < 2$) at IT–HS conditions is a combination of subgrain rotation recrystallization, glide-induced vorticity, grain boundary migration, with subordinate activity of spontaneous nucleation and rigid body rotation (Fig. 8b). The rotation of intracrystalline glide planes towards an orientation favouring slip parallel to the SZB (Fig. 3) is associated primarily with progressive subgrain rotation recrystallization, leading to a strong decrease in the average grain size (Figs. 6 and 7). Rigid body rotation of grains is unimportant compared to the HT–HS experiments. The grain SPO forms a similar angle with the SZB (60°) as those observed in the high-temperature experiments and this angle becomes strain invariant already during the first transient stage. Herwegh and Handy (1996) related this angle to the average 60° angle between the SZB and dominant microshear zones within the sample (see also Herwegh and Handy, 1997). A weak domainal microfabric consisting of yellow and magenta grains develops at the end of this stage (Figs. 3 and 5c). As in the high-temperature experiments, a symmetrical c-axis cross girdle forms perpendicular to the long axis of the finite strain ellipse calculated for the entire sample (Fig. 3).

3.2.2. Second transient stage

With progressive deformation, a combination of subgrain rotation, glide-induced vorticity and grain boundary migration strengthen the domainal microfabric (Fig. 3). In particular, we noticed that noncoaxial shearing of grain boundary bulges rotates these bulges into parallelism with the grain boundaries. Renewed bulging along these sheared boundaries contributes to the growth of domains (see fig. 10 in Herwegh and Handy, 1996). The average width of these domains (170 μm) is less than the domain width in the high-temperature experiments. The average grain size still decreases during the second transient stage due to the continued activity of subgrain rotation recrystallization and spontaneous nucleation (Figs. 6 and 7). We apply the term 'spontaneous nucleation' to the sudden appearance of minute grains in animated digital images of the evolving microstructure. These grains grow rapidly at the expense of other grains until attaining dimensions comparable to those of optical subgrains. It is unclear if their nucleation involves the progressive rotation of TEM-size subgrains, the rotation of small grain fragments, or even classical nucleation (Drury and Urai, 1990). We favour the first possibility, however, because spontaneous nucleation tends to occur together with subgrain rotation recrystallization near the boundaries of larger host grains (e.g., Fig. 8a,b). The microfabric is completely recrystallized at shear strains greater than 4. During the second transient stage, the c-axis cross girdle rapidly reduces to an oblique single girdle (last two columns of Fig. 3). Interestingly, several small cracks opened perpendicular to the incremental stretching axis. These cracks lengthened as they rotated synthetically into parallelism with the main axis of the finite strain ellipse (compare with LT–HS experiments below).

3.2.3. Steady state

At $\gamma > 6$, grain size, domain width, grain SPO, and texture all become invariant with strain on the sample scale (Figs. 3 and 5c). On the grain scale, however, subgrain rotation and the cyclical growth and consumption of individual grains or subgrains constantly 'refreshes' the microfabric (see Fig. 8b). The elongate fractures that formed and rotated during the second transient stage remain open parallel to the main axis of finite strain ellipse. Compared to the high-temperature microstructures, the IT–HS steady state microstructure shows a much smaller average grain size (Figs. 6 and 7), a smaller domain width (Figs. 2 and 3), a steeper SPO, a different mechanism assemblage and other relative mechanism activities (Fig. 8). These pronounced differences between high- and intermediate-temperature microstructures are also manifest in the steady-state textures: point c-axis maxima typical of high-temperature deformation are replaced by oblique c-axis single girdles with a stable obliquity with respect to the SZB at shear strains greater than 6 (right-hand column in Fig. 3).

Natural equivalents to the IT–HS norcamphor microstructures are rather common in greenschist facies quartz mylonites (e.g., Knipe and Law, 1987; Law et al., 1990) and have also been generated in both coaxial shear (regime 3 microstructures of Hirth and Tullis, 1992) and split cylinder shear experiments on quartzite (Dell'Angelo and Tullis, 1989). In the experiments by Hirth and Tullis (1992), quartz also begins to recrystallize along the boundaries of host grains by a combination of subgrain rotation and grain boundary migration recrystallization. At strains corresponding to 57% axial shortening, complete recrystallization of the sample eradicated all vestiges of the core–mantle structure in quartz (see fig. 6d in Hirth and Tullis, 1992). Spontaneous nucleation and veining such as observed in the norcamphor experiments were not reported from any of the quartz experiments in the literature. Identical textures to the IT–HS norcamphor textures documented in Fig. 3 can be found in natural quartz aggregates that were subjected to plane strain simple shearing under greenschist to lower amphibolite facies conditions (Schmid and Casey, 1986; Law et al., 1990). In quartz, this type of texture pattern is interpreted to reflect slip on the prism, basal and rhomb planes in the $\langle a \rangle$ direction.

3.3. Low temperature–high strain rate (LT–HS) experiments

3.3.1. First transient stage

An oblique ribbon grain SPO develops already during the first increments of shear strain. This reflects a significant component of glide-induced vorticity (Fig. 4). Compared to the previous experiments, dynamic recrystallization is strongly suppressed and involves limited grain boundary migration (Figs. 4 and 8). The texture comprises a symmetrical c-axis cross girdle (Fig. 4).

During this low-temperature crystal plasticity, fractures develop along grain boundaries with an initial orientation of 135° to the SZB, i.e. parallel to the inferred σ_1 direction of simple shear (Fig. 9). With continued strain, the following two types of crack evolution can be discerned:

(1) Cracks open parallel to the incremental stretching direction and propagate parallel to the σ_1 direction. They then interconnect to form a big vein that truncates the entire shear zone (white crack labelled 2 in Fig. 9). Pinning of such veins at the SZB prevents their rotation during the simple shearing experiment.

(2) In cases where cracks do not interconnect, they remain relatively small and rotate synthetically into concordance with the SZB. The cracks open as long as their long axes lie within the shortening field, but close obliquely upon rotation into the extensional field. Once the cracks are closed, only a few bubble trails subparallel to the long axis of the finite strain ellipse mark the former location of the cracks (see bubbles labelled 1 in Fig. 9).

3.3.2. Second transient stage

Dynamic recrystallization involving a combination of subgrain rotation recrystallization and grain boundary migration typifies this stage. This is associated with a reduction in the average grain size and the development of a core–mantle structure (Figs. 4, 6 and 7). The large veins continue to dilate, but no new fractures nucleate in the norcamphor between

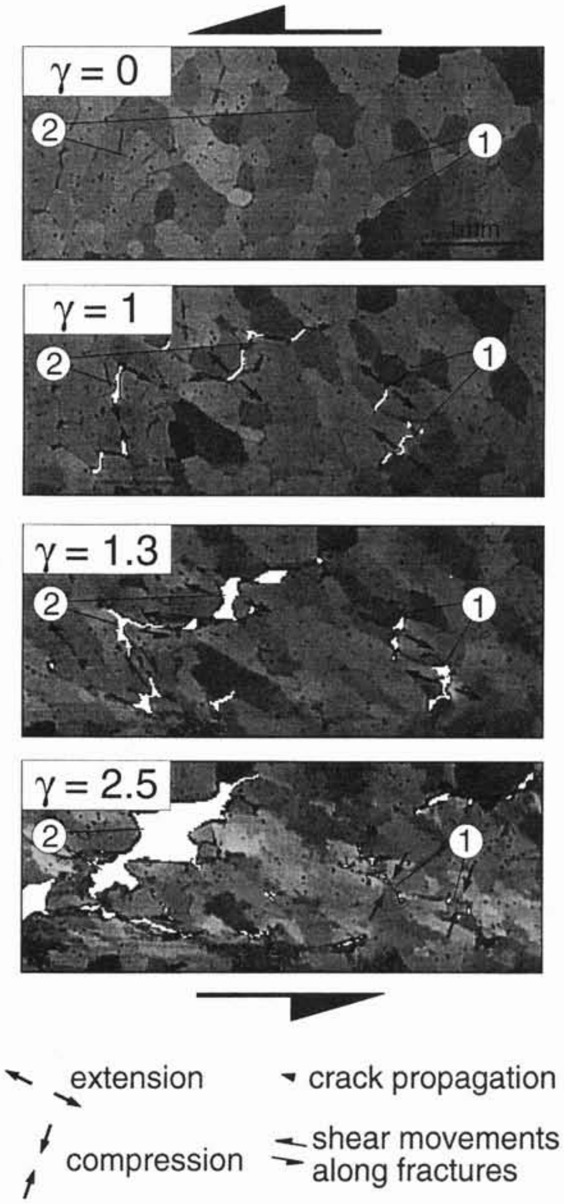

Fig. 9. Crack evolution in the sample deformed at LT–HS conditions. Type 1 cracks nucleate at grain boundaries oriented 135° to the SZB. They then open and rotate synthetically towards the SZB. These cracks close upon rotation into the shortening field of the incremental strain ellipse (0–90° to SZB). Note bubbles outlining the trace of the closed crack. Type 2 cracks nucleate as above, propagate perpendicular to the incremental stretching direction and interconnect to form a big vein.

the fractures. A *c*-axis texture develops in uncracked regions, suggesting that intracrystalline glide and dynamic recrystallization are able to maintain strain compatibility in the parts of the aggregate between the cracks. Thus, the localized cracking does not appear to have a strong influence on texture evolution, at least at low strains.

It is important to note that close spatial and temporal relationship of microstructures related to fracturing and intracrystalline plasticity is a diagnostic criterion for the brittle to crystal plastic transition in natural fault rocks (i.e. 'frictional to viscous transition' of Schmid and Handy, 1991). Although synmylonitic cracks have been recognized in greenschist facies quartz mylonites (e.g., plates 4.20 and 4.22 in Handy, 1986), the big cracks formed in the LT–HS norcamphor experiment are probably not very realistic. The unrealistically low confining pressure in our experiment favours the opening of such cracks. Moreover, because these cracks are pinned at the SZB, they cannot all rotate into an orientation which would lead to their closing. Finally, the lack of a fluid phase in the experiments inhibits sealing of the cracks via solution–precipitation mechanisms. Unfortunately, the inability of the big cracks to rotate and seal lead to disintegration of the sample, preventing us from reaching shear strains of greater than 5 in the LT–HS experiments. Therefore, steady state was never attained.

To summarize this section, our experiments indicate that microfabric evolution in norcamphor is highly temperature- and strain-rate-dependent. Fig. 8d shows the relationship between the temperature–strain rate conditions and the dominant grain scale mechanism inferred from the microfabrics in our experiments. Shearing of norcamphor at high homologous temperatures favours grain boundary migration recrystallization as the dominant grain scale mechanism accommodating glide-induced vorticity within the aggregate. Increasing strain rate at this high temperature tends to increase the relative activity of subgrain rotation recrystallization and, at low strains, also to favour rigid body rotation of 'hard grains' (i.e. grains poorly oriented for slip parallel to the SZB). By comparison, microfabrics generated in simple shear at an intermediate homologous temperature are much finer grained, indicating the predominance of subgrain rotation recrystallization. In experiments conducted at the lowest homologous temperatures, the inability of crystal plastic mechanisms such as intracrystalline glide and dynamic recrystallization to accommodate the bulk strain compatibly leads to the opening of tensional cracks along grain boundaries. The aggregate deforms at the brittle to ductile transition. In all experiments, however, the microstructural changes are strongly linked to a textural evolution characterized by the transition from a symmetrical c-axis cross girdle to an oblique c-axis single girdle with respect to the long axis of the finite strain ellipse. In the next section, we examine the way in which the rotational history of individual grains relates to the formation and preservation of a steady state microfabric.

4. Crystallographic rotation paths and rates

The texture of a polycrystalline aggregate comprises grains with different crystallographic orientations and rotation histories. Up to now, such rotational histories could only be approximated by measuring the crystallographic axes on the U-stage once the experiments were stopped (Jessell, 1986; Herwegh and Handy, 1996) or by inserting a Berek compensator during experimental runs to intermediate shear strains ($\gamma = 1.4$, in Ree, 1991). We therefore applied the CIP method (described above) during the HT–LS runs to record a sufficiently dense orientation image distribution per shear strain increment to calculate the rotation paths of individual grains.

Basically three different types of rotational path can be observed in the pole figures in Fig. 10a,b: type I, shallowly inclined c-axes at the periphery that rotate synthetically with respect to the bulk sense of vorticity; type II, steeply inclined c-axes that remain in the centre of the pole figures; and type III, intermediate to steep c-axes in the centre of the pole figures that rotate towards smaller inclinations. These general c-axis paths are shown schematically in Fig. 11a. The relative rates of the orientational changes corresponding to these three types of rotational paths are best seen in those parts of Fig. 10 that depict changes in the azimuth (Fig. 10c,d) and inclination (Fig. 10e,f) of norcamphor c-axes as a function of shear strain. The steeper the curve, the faster the rate of crystallographic rotation. Therefore, grains with paths types I and II correspond to the flat curves in Fig. 10e,f, indicating a low rate of inclinational change, whereas grains with path type III have steep curves diagnostic of high rates of inclinational change. Interestingly, there is no general correlation between grains' orientational path type and changes in azimuth in Fig. 10c,d. Some grains maintain their azimuth (flat curves) whereas others show initially high rates of azimuth change that decrease with strain (concave curves in Fig. 10c,d).

This rather complex relationship between crystallographic orientation and rotation rate is summarized in Fig. 11b, which outlines fields of relative c-axis orientational stability (= low c-axis rotation rates). The boundaries of the stability fields in this diagram derive directly from the angles corresponding to horizontal dashed lines that separate differently sloped curves in Fig. 10c–f. c-axes with orientations in the white field of Fig. 11b rotate quickly toward orientations with slower rotation rates (hatched fields in Fig. 11b) before being eliminated by dynamic recrystallization (short curves between dashed lines in Fig. 10c–f, e.g., grains 2, 5, 14, 18). Intersections of the left- and right-hatched fields in the pole figure correspond to the relatively narrow range of axial orientations that are characterized by low azimuthal and inclinational rotation rates. It is probably not coincidental that these fields of relatively high axial stability also contain the c-axis point maxima making up the bulk texture in norcamphor at intermediate to high shear strains (shaded elliptical areas in Fig. 11, recall Fig. 2). Also, newly nucleated grains usually show c-axis orientations within, or at least very close to, the field of maximum orientational stability in Fig. 11b (e.g., grains 19, 25, 27, 30 in Fig. 10).

The distribution of the orientational stability fields in Fig. 11b bears implications for the evolution of texture on the scale of the entire norcamphor sample. The symmetrical c-axis cross girdle that forms at low to intermediate simple shear strains in the first transient stage of the HT–LS experiments (Fig. 2; $\gamma = 2$) consists of grain orientations in the low rotational rate fields of Fig. 11b. As mentioned above, these rotations primarily involve glide-induced vorticity (Fig. 8a). In analogy with quartz, slip is inferred to occur both on the prism $[m]$ slip system and on conjugate basal glide planes in the $\langle a \rangle$ direction (discussion in Herwegh and Handy, 1996). This allows

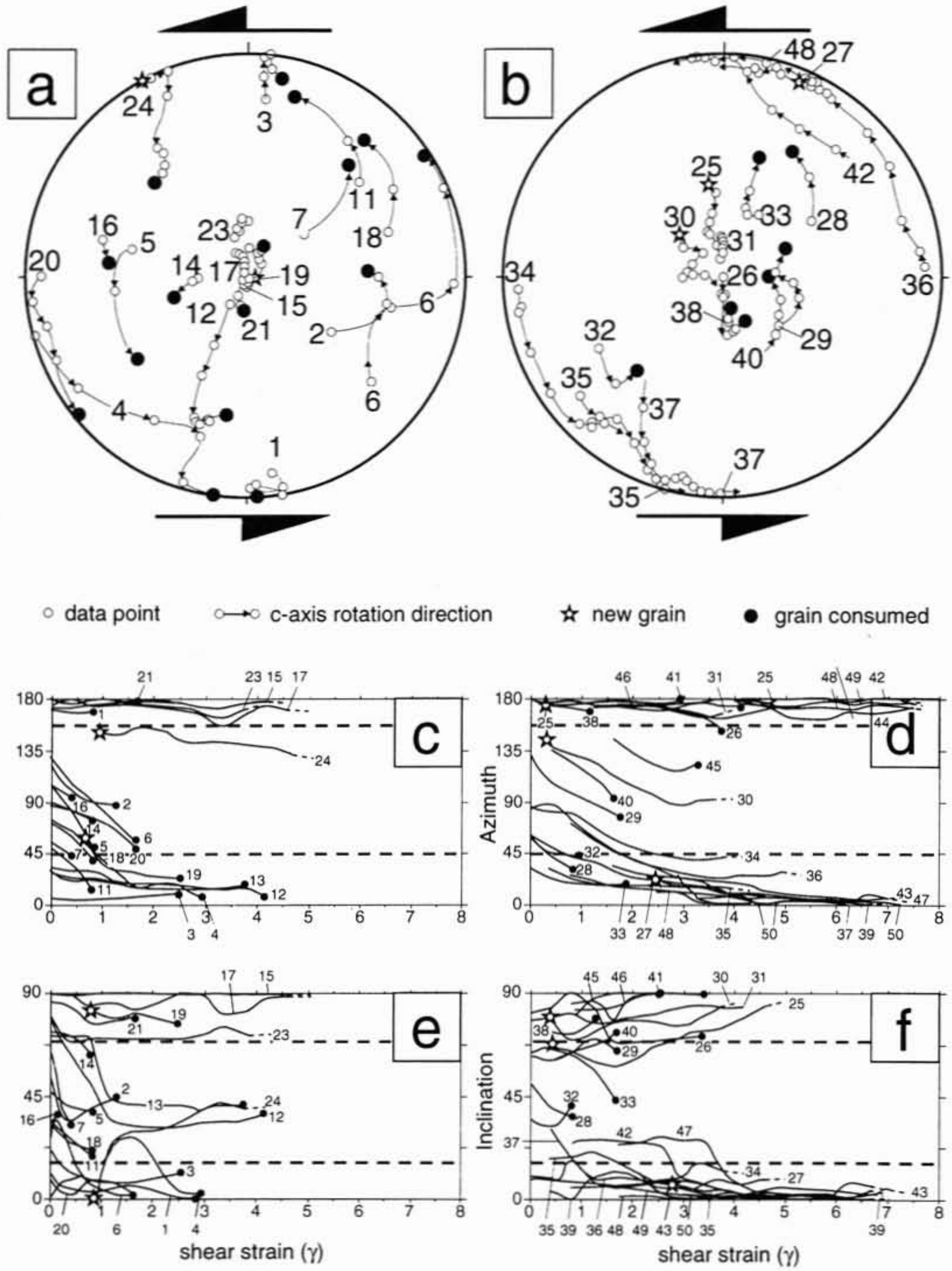

Fig. 10. c-axis rotation paths for individual grains. Equal-area pole figures showing c-axis rotation paths of individual grains (a, b). Azimuth vs. shear strain diagrams (c, d). Inclination vs. shear strain diagrams (e, f). To aid visualization of the c-axis rotational histories, orientations from opposite quadrants of the pole figures are combined so that only a 180° azimuth range is depicted on the vertical axes of (c) and (d). This is justified by the symmetry of most c-axis rotational paths with respect to the centre of the pole figures. Dashed horizontal lines in (c) to (f) delineate orientational stability domains depicted in Fig. 12 (see text for explanation).

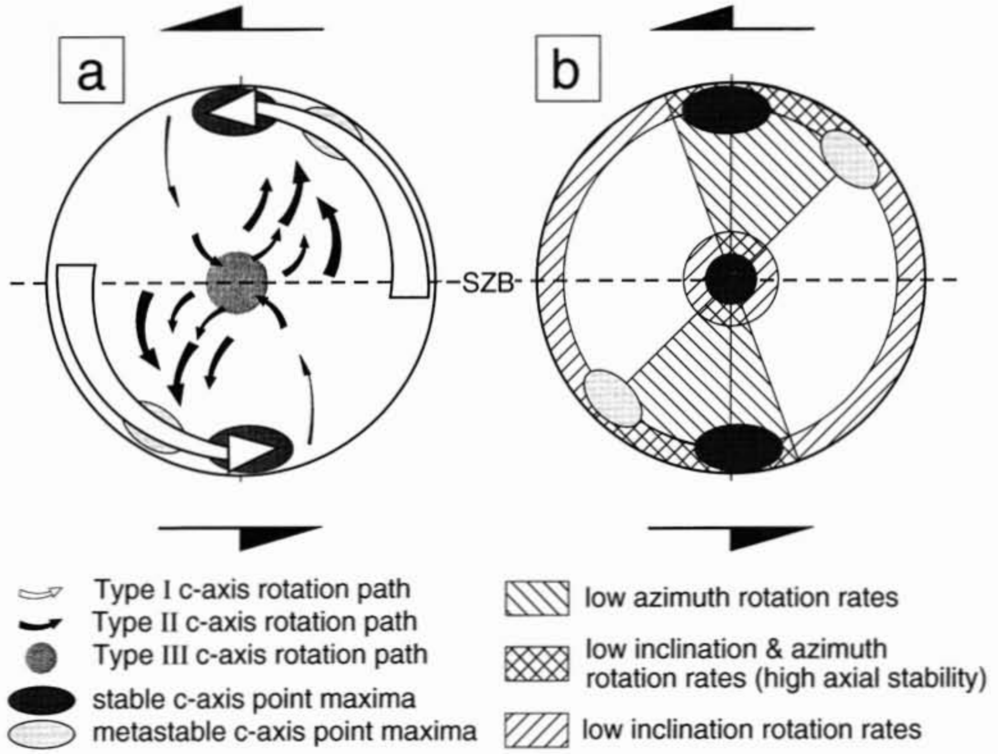

Fig. 11. (a) Three general types of *c*-axis rotation paths derived from pole figures in Fig. 10a,b. (b) Pole figures showing fields of varied *c*-axis rotation rates (see text for explanation).

pure shear extension of the norcamphor aggregate parallel to the long axis of the finite strain ellipse. Why does such a seemingly stable cross girdle texture yield to the *c*-axis single girdle in the second transient stage? A glance at the *c*-axis trajectories at the periphery of the pole figures in Fig. 10a,b provides a possible explanation: grains that have attained an orientation in the peripheral high stability field (Fig. 11b) continue to rotate at a low rate synthetically with respect to the bulk sense of vorticity (e.g., grains 4, 6, 20 in Fig. 10). As shown in Fig. 5a, the volume proportion of such grains (violet and magenta grains) decreases dramatically at shear strains between 2 and 4 due to the increased relative activity of grain boundary migration recrystallization (see also Fig. 8a). This slow rotation of individual grains' *c*-axes in the presence of syntectonic grain boundary migration continues, with the *c*-axes of most surviving grains attaining an orientation coincident with the steady state point maxima (e.g., grains 35, 36 in Fig. 10). Up to steady state, the crystallographic rotation of individual grains is accompanied by a slight synthetic rotation of the single girdle skeletal outline with respect to the SZB (textures for $\gamma = 4$ to 6 in Fig. 2).

At steady state, rotation of the peripheral point maxima with respect to the SZB stops, but the *c*-axes of individual grains within the aggregate continue to rotate. This is shown in Fig. 12, which contains an orientation image sequence through an orientational slice (azimuth ranges 170–190° and 350–010° at inclinations of 0° to 10°) corresponding to the peripheral *c*-axis point maxima for the steady state HT–LS texture. In this figure, the grey tones correspond to 2° intervals within this azimuth range (see upper left-hand corner of Fig. 12). Deformation bands and prismatic subgrains in Fig. 12 have low-angle boundaries (2–10°) that are oriented subperpendicular to the SZB. Both the boundaries and the *c*-axes of the subgrains rotate synthetically (see deformation band labelled 1 in Fig. 12 and progressively darkening subgrain to the left of this band). This rotation

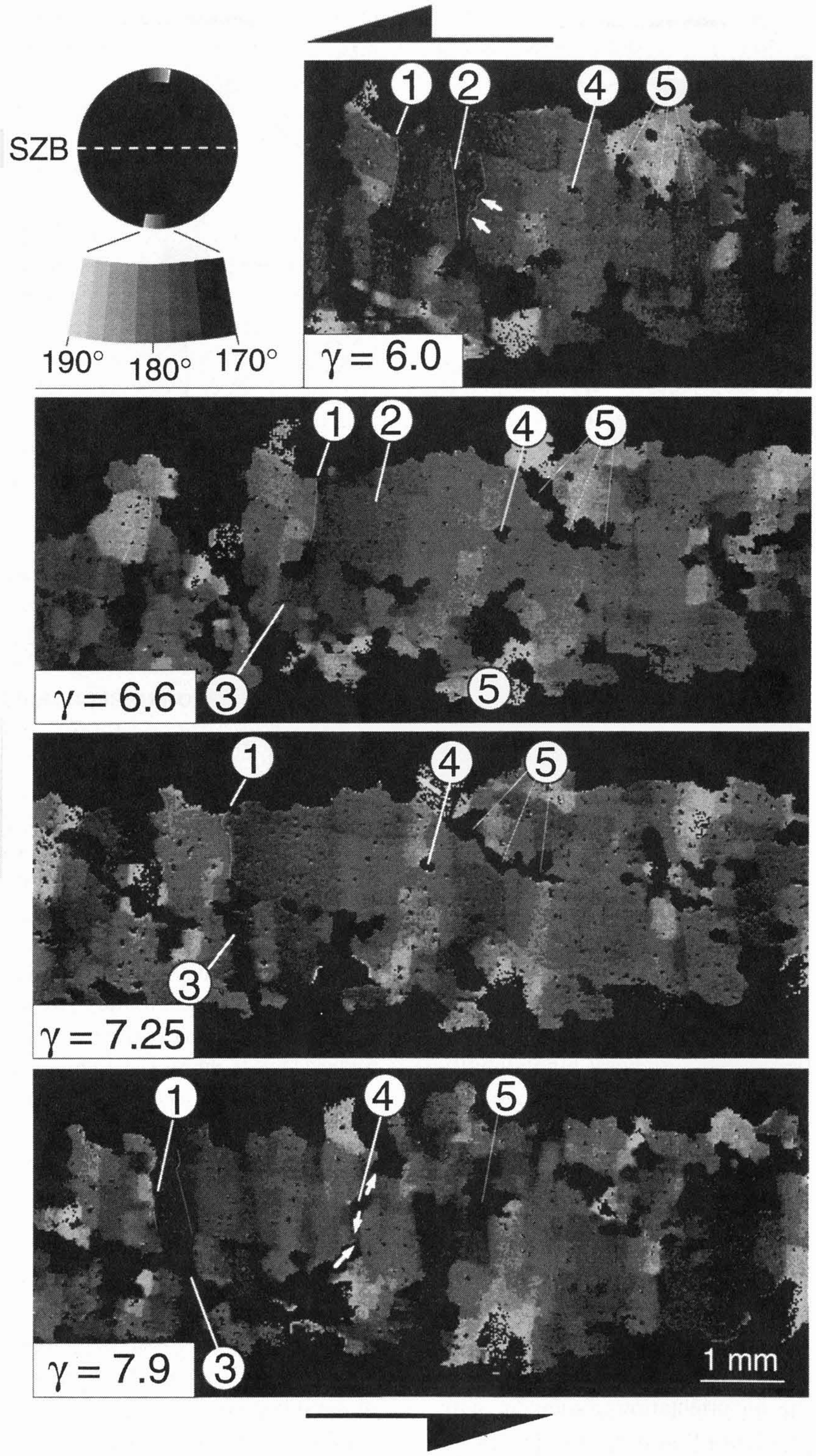

Fig. 12. Changes in crystallographic orientation and microstructure in a steady state HT–LS experiment. Pole figure in the upper left-hand corner shows the grey tones corresponding to 2° azimuth intervals for flat-lying *c*-axes within the peripheral steady state point maxima (see text for further explanation).

continues until the subgrains are consumed by one of two mechanisms: (1) low-angle grain boundary migration of adjacent subgrains whose basal planes are oriented subparallel to the SZB (subgrain labelled 2 in Fig. 12); or (2) high-angle grain boundary migration of neighbouring grains (grain labelled 4 in Fig. 12). A few grains even manage to rotate out of the favourable slip orientation before being consumed (see grain labelled 3 in Fig. 12). The rotation path of such grains is similar to that of grain 24 in Fig. 10a. Most black grains in Fig. 12 are favourably oriented for prism glide, as inferred from their *c*-axis orientations parallel to the *Y* fabric direction (steady state point maximum at the centre of the pole figures in Fig. 2). The black grain cluster labelled 5 in Fig. 12 undergoes cyclical growth, coalescence, grain size reduction, and dismemberment during grain boundary migration recrystallization. Thus, the continuous rotation of crystallographic axes observed on the grain scale is not perceived on the sample scale because grain boundary migration usually consumes grains whose predominant slip planes rotate out of an easy glide orientation. It is interesting to note the similarity of this behaviour with that predicted by the twinned fibre domain model by Cobbold and Gapais (1986). In their model, slip domain boundaries rotate and migrate until slip is accommodated primarily (but not exclusively) along planes oriented parallel to the SZB (see their combined modes I and II). This demonstrates the importance of dynamic recrystallization in preserving steady state textures.

5. Effect of temperature and strain rate on texture

In all experiments, simple shearing is associated with the formation of a symmetric *c*-axis cross girdle that is progressively replaced by a rotating, oblique *c*-axis single girdle, which at steady state either stabilizes (IT–HS experiments) or yields to a stable *c*-axis point maxima (HT–LS and HT–HS experiments; see Fig. 13). Despite the similarity of these bulk textures, the details of crystallographic rotation histories are inferred to vary between the experiments due to differences in the grain scale mechanism assemblage. The maximum density of orientation images per strain increment in the IT–HS and LT–HS experiments was too low to enable us to track the *c*-axes of norcamphor grains, but the general similarity both of the textures and of their strain-dependent transitions in Fig. 13 leads us to believe that the general concept of rotational stability fields (recall Fig. 11b) applies to norcamphor in all of the experiments. Slight differences in the geometry of the textures suggest that the relative size of these stability fields varies with the extrinsic conditions of simple shearing. For example, Fig. 14 shows that the opening angle between the two legs of the *c*-axis cross girdle (Fig. 13) is smaller at lower temperatures and higher strain rates than in the HT–LS experiments. Similar temperature-dependent variations in this angular relationship have also been observed in *c*-axis cross girdle patterns from high-grade quartz mylonites (Behr, 1968), ostensibly deformed under coaxial conditions (Lister and Dornsiepen, 1982). This indicates that the fields of the relatively fast crystallographic rotation in Fig. 11b (white areas) increases at the expense of the low rotational rate fields with increasing temperature and/or decreasing strain rate. We attribute this to the observed increase in the relative activity of subgrain rotation recrystallization at lower temperatures (compare microstructures in Figs. 2 and 3; see also Fig. 8).

The asymmetry of the single and cross girdles with respect both to the main foliation, Sa, and the SZB changes as a function of shear strain in all the experiments (Fig. 13). This is seen more clearly in Fig. 15, where the angle β between the SZB and the central segment of the *c*-axis skeletal outlines decreases with progressive shear strain. In order to visualize the relative rates of textural rotation and passive material rotation within the sample, Fig. 15 also contains a solid curve representing the angle between the short axis of the finite strain ellipse and the SZB. The rotation rate of the *c*-axis cross girdles during the first transient stage coincides approximately with that of the finite strain ellipse. During the second transient stage ($\gamma = 2$ to 6), however, the textural rotation rate increases abruptly as the texture changes from a cross girdle to a single girdle pattern. This has also been observed during simple shear deformation of olivine aggregates (fig. 4 in Zhang and Karato, 1995). Note that the cross girdle to single girdle transition in norcamphor generally occurs at lower strains for higher temperatures, presumably

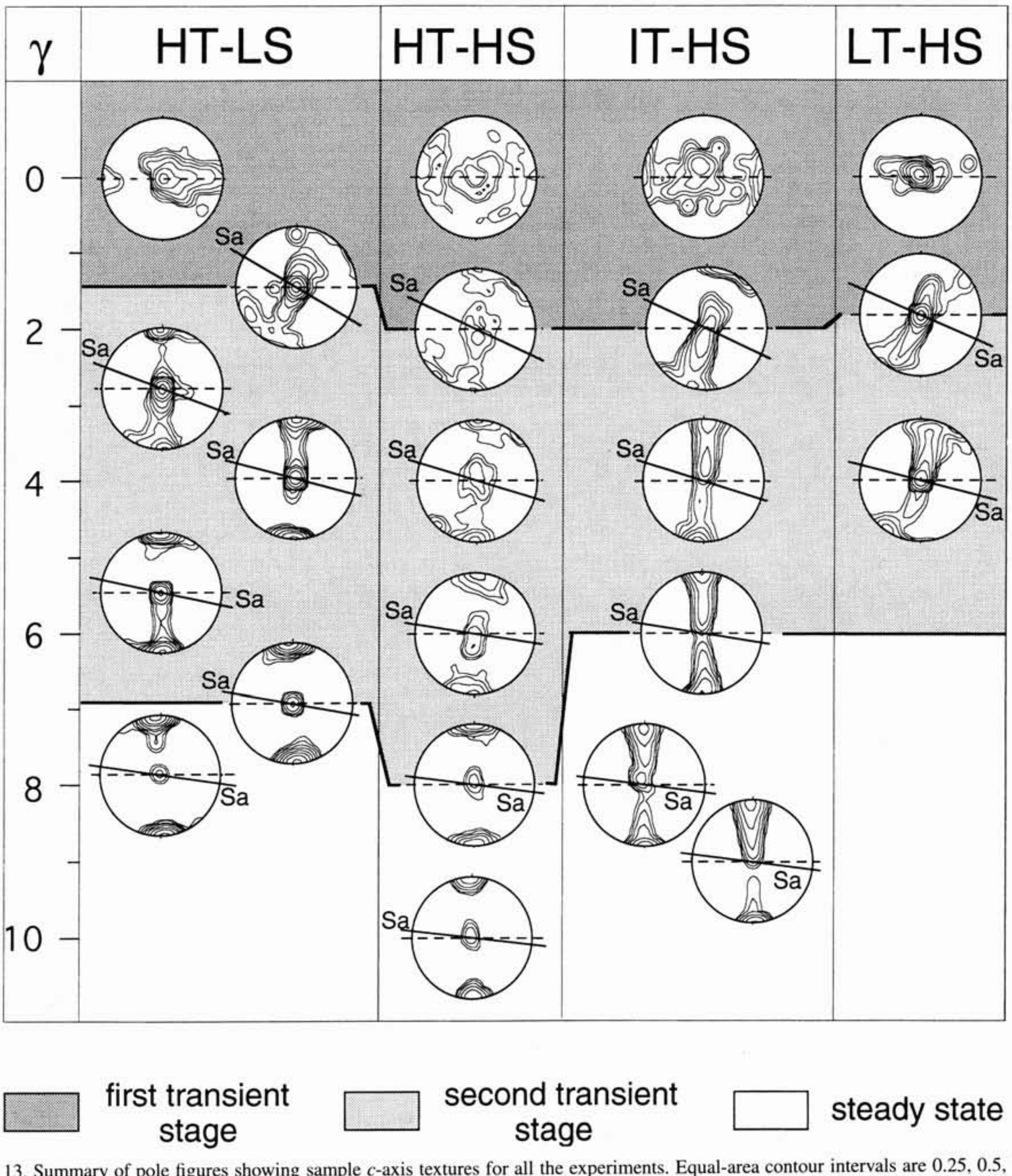

Fig. 13. Summary of pole figures showing sample *c*-axis textures for all the experiments. Equal-area contour intervals are 0.25, 0.5, 1, 4, 8, 16, 32 times uniform distribution for the HT–LS, IT–HS, and LT–HS experiments, contour intervals are 1, 2, 4, 8, 16 times uniform distribution for the HT–HS experiments. Dashed lines represent the shear zone boundary (SZB); *Sa*, refers to the long axis of the finite strain ellipse.

due to the higher relative activity of grain boundary migration recrystallization in the high-temperature experiments (Fig. 8). At steady state, the textures stop rotating and the β angle stabilizes at values of 86–88°. The sample textures have attained a stable end orientation with respect to the SZB.

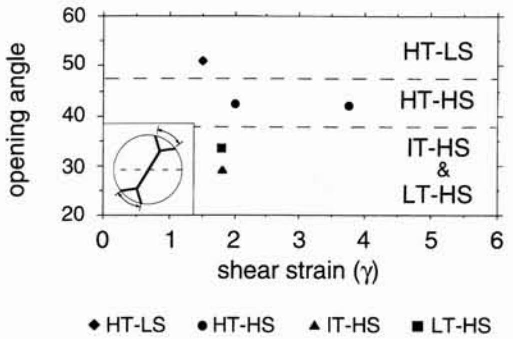

Fig. 14. Temperature and strain rate dependence of the opening angle between legs of the *c*-axis cross girdles in Fig. 13.

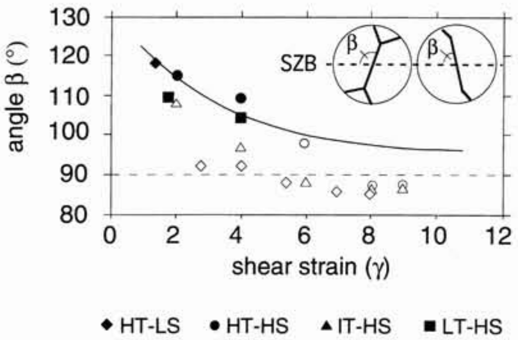

Fig. 15. Textural obliquity with respect to the SZB (angle β) vs. shear strain at different experimental conditions. Solid curve is the angle between the short axis of the finite strain ellipse and the SZB. Filled and open symbols represent the main limbs, respectively, of the cross girdles and single girdles. Dashed line at 90° depicts the normal to the SZB.

6. Resolution of a long-standing debate?

The results of the textural analysis presented above may shed some new light on the controversy regarding texture evolution outlined in the introduction. Before discussing the norcamphor experiments in this context, it is important to consider the different approaches underlying the stable end orientation and ideal orientation concepts. Implicit in the concept of a stable textural end orientation is the notion that slip systems in the grain aggregate rotate until they attain an orientation that maximizes the resolved shear stress in the slip direction (i.e. the easy glide orientation; Schmid and Casey, 1986). In accordance with the modelling work of Etchecopar (1977) and Etchecopar and Vasseur (1987), these planes are then assumed to maintain this stable, irrotational orientation with respect to the SZB during further strain (e.g., p. 37 in Law et al., 1990). Therefore, the stable texture of an aggregate at steady state is believed to reflect a stationary orientation of the individual grains making up the aggregate. In contrast, the ideal orientation concept involves explicit assumptions about the way in which strain compatibility is maintained within the aggregate in order to generate a model texture. As stated in the Introduction, most models that invoke the ideal orientation concept neglect dynamic recrystallization (except for Jessell, 1988a,b; Jessell and Lister, 1990) and assume either uniform strain (Lister et al., 1978) or average (i.e. self-consistent) strain within the aggregate (Wenk et al., 1989). These assumptions lead to discontinuously rotating slip systems. In quartz, this is associated with point maxima whose obliquity with respect to the SZB appears to be opposite to that observed in nature and experiment (e.g., see fig. 9 in Wenk and Christie, 1991).

Our norcamphor experiments suggest that although both approaches explain certain aspects of texture formation, neither approach is entirely valid. While the experimental textures certainly attain a stable end orientation on the scale of the norcamphor samples, the slip systems of individual grain are not stationary at steady state and can even undergo a limited amount of rotation out of easy glide orientations before being consumed by neighbouring grains during dynamic recrystallization. In fact, dynamic recrystallization plays a central role in maintaining strain compatibility within a polycrystalline aggregate deforming at high strains, as Schmid (1994) and co-workers (Schmid and Casey, 1986; Schmid et al., 1987) have already noted. In addition, previous experiments in norcamphor (Herwegh and Handy, 1996) have shown that microshearing on the supragranular scale within the aggregate contributes to maintaining strain compatibility on the granular scale. Both of these effects should be incorporated into future modelling of polycrystalline aggregates.

We end this section on a semantic note by recommending that the term 'stable end orientation' be applied only to bulk textures at steady state. Only on the bulk (i.e. aggregate) scale is the crystallographic orientation of grains statistically invariant with strain and time. This term should be avoided, however, when describing the crystallographic behaviour of individual grains or subgrains within an aggregate, because the microfabric studies above show that steady state on the granular scale is both heterogeneous and dynamic, involving the cyclic growth, rotation and consumption of individual grains.

7. Geological applications

The microfabrics generated in the norcamphor experiments described above bear directly on the way in which quartz microstructures can be used in field studies. Fig. 16 shows that no sense of shear can be derived at low shear strains unless the SZB is exposed, because the grain SPO and the *c*-axis cross girdle pattern are symmetrically disposed with respect both to each other and to the main foliation, Sa. At intermediate to high shear strains, however, the obliquity of the skeletal outline of cross or single girdles with respect to the main foliation, as well as the pronounced SPO in dynamically recrystallized aggregates, are both good kinematic indicators (see also Burg and Laurent, 1978; Simpson, 1980; Simpson and Schmid, 1983). Note that symmetrical cross girdle patterns form during the first transient stage of simple shearing and do not necessarily indicate an overall regime of coaxial flow (Hudleston, 1978; Bouchez and Duval, 1982; Herwegh and Handy, 1996).

The microfabrics and mechanism assemblages can also be used to make qualitative inferences about temperature and strain rate. In general, a predominance of grain boundary migration recrystallization is diagnostic of high homologous temperature, whereas subgrain rotation recrystallization indicates relatively low homologous temperature and/or high strain rate. A similar dependence of dynamic recrystallization mechanism on temperature and strain rate has been inferred for deformed minerals (e.g., quartz, Schmid and Casey, 1986; calcite, Schmid et al., 1987) and inorganic rock analogues (magnesium, Drury et al., 1985; sodium nitrate, Tungatt and Humphreys, 1981).

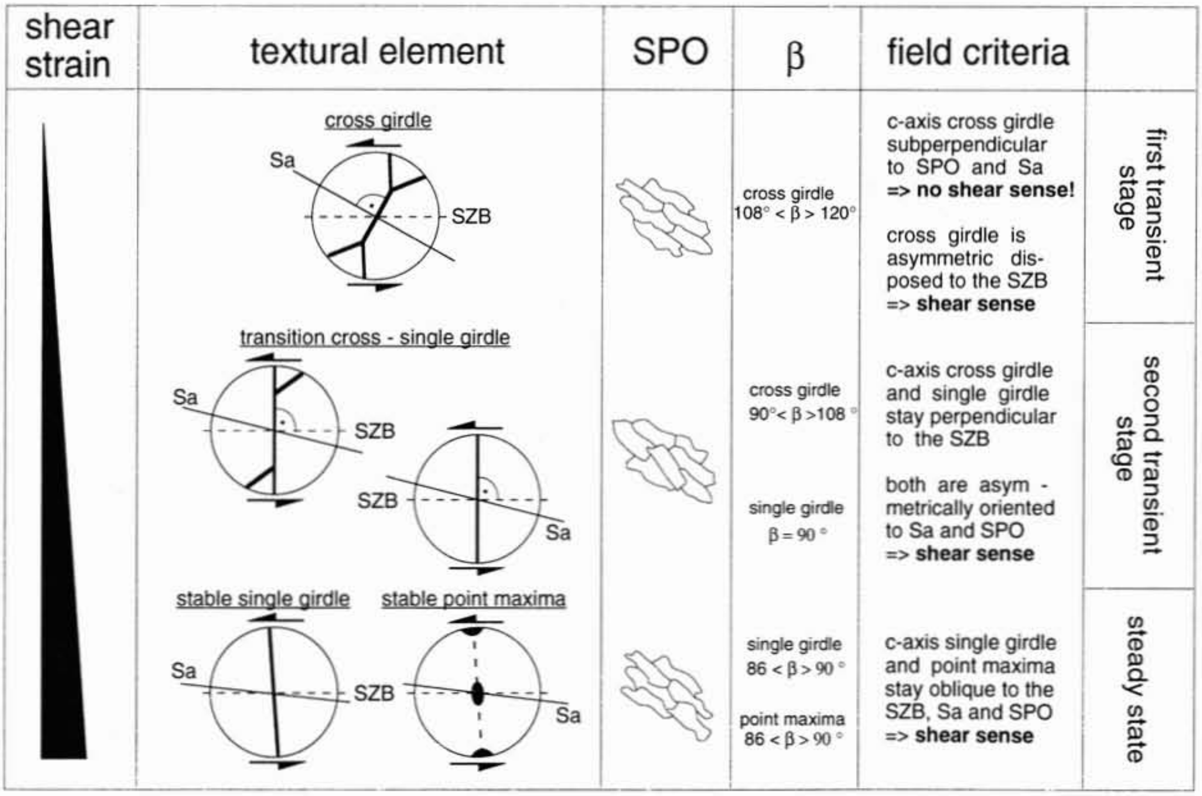

Fig. 16. Field criteria for shear sense determination in mylonitic quartz-bearing rock at different shear strains.

Finally, we point out that the experimental deformation of rock analogues is no substitute for careful experimentation on real mineral aggregates. In particular, further studies are needed to see if our observations and inferences also hold for hexagonal minerals such as quartz or ice. Only the calibration of the basic textural and microstructural relationships observed in in situ experiments can improve the application of microstructures to solving geologic problems.

Acknowledgements

We wish to thank Tectonophysics reviewers C. Passchier and Anonymous for their helpful comments. The financial support of the Swiss National Science Foundation in the form of project grants 21-30598.91 and 21-33814.92 to Mark Handy and grant 21-36008.92 to Renée Heilbronner is acknowledged with gratitude.

References

Behr, H.J., 1968. Zur tektonischen Analyse magmatischer Körper unter besonderer Berücksichtigung des Quarzkorngefüges, I. Freiberger Forsch. C215, 9–59.

Bons, P.D., 1993. Experimental deformation of polyphase rock analogues. Geol. Ultrajectina 110, 207 pp.

Bouchez, J.L., Duval, P., 1982. The fabric of polycrystalline ice deformed in simple shear: experiments in torsion, natural deformation and geometrical interpretation. Text. Microstruct. 5, 171–190.

Burg, J.P., Laurent, Ph., 1978. Strain analysis of a shear zone in a granodiorite. Tectonophysics 47, 15–42.

Burg, J.P., Wilson, C.J.L., Mitchel, J.C., 1986. Dynamic recrystallization and fabric development during simple shear deformation of ice. J. Struct. Geol. 8, 857–870.

Cobbold, P.R., Gapais, D., 1986. Slip system domains, 1. Plane strain kinematics of arrays of coherent bands with twinned fibre orientations. Tectonophysics 131, 113–132.

Dell'Angelo, L.N., Tullis, J., 1989. Fabric development in experimentally sheared quartzites. Tectonophysics 169, 1–21.

Drury, M.R., Urai, J.L., 1990. Deformation-related recrystallization processes. Tectonophysics 172, 235–253.

Drury, M.R., Humphreys, F.J., White, S., 1985. Large strain deformation studies using polycrystalline magnesium as a rock analogue, II. Dynamic recrystallization mechanism at high temperatures. Phys. Earth Planet. Inter. 40, 208–222.

Etchecopar, A., 1977. A plane kinematic model of progressive deformation in a polycrystalline aggregate. Tectonophysics 39, 121–139.

Etchecopar, A., Vasseur, G., 1987. A 3-D kinematic model of fabric development in polycrystalline aggregates: comparison with experimental and natural examples. J. Struct. Geol. 9, 705–717.

Handy, M.R., 1986. The Structure and Rheological Evolution of the Pogallo Fault Zone, a Deep Crustal Dislocation in the Southern Alps of Northwestern Italy (Prov. Novara). Unpublished Ph.D. Thesis, Univ. of Basel, 327 pp.

Herwegh, M., 1996. Microfabric Evolution in Monomineralic Mylonites: An Experimental Approach Using See-Through Analogue Materials. Unpublished Ph.D. Thesis, Univ. of Berne.

Herwegh, M., Handy, M.R., 1996. The evolution of high temperature mylonitic microfabrics: evidence from simple shearing of a quartz analogue (norcamphor). J. Struct. Geol. 18, 689–710.

Herwegh, M., Handy, M.R., 1997. The origin of shape preferrred orientations in mylonite: inferences from in-situ experiments on polycrystalline norcamphor. J. Struct. Geol., submitted.

Hirth, G., Tullis, J.T., 1992. Dislocation creep regimes in quartz aggregates. J. Struct. Geol. 14, 145–159.

Hudleston, P.J., 1978. Progressive deformation and development of fabric across zones of shear in glacial ice. In: Saxena, S., Bhattacharji, S. (Eds.), Energetics of Geological Processes. Springer Verlag, Berlin, pp. 121–150.

Jessell, M.W., 1986. Grain boundary migration and fabric development in experimentally deformed octachloropropane. J. Struct. Geol. 8, 527–542.

Jessell, M.W., 1988a. Simulation of fabric development in recrystallizing aggregates, I. Description of the model. J. Struct. Geol. 10, 771–778.

Jessell, M.W., 1988b. Simulation of fabric development in recrystallizing aggregates, II. Example model runs. J. Struct. Geol. 10, 779–793.

Jessell, M.W., Lister, G.S., 1990. A simulation of the temperature dependence of quartz fabrics. In: Knipe, R.J., Rutter, E.H. (Eds.), Deformation Mechanisms, Rheology and Tectonics. Geological Society, London, pp. 353–362.

Knipe, R.J., Law, R.D., 1987. The influence of crystallographic orientation and grain boundary migration on microstructural and textural evolution in an S–C mylonite. Tectonophysics 135, 155–169.

Law, R.D., Schmid, S.M., Wheeler, J., 1990. Simple shear deformation and quartz fabrics: a possible natural example from the Torridon area of NW Scotland. J. Struct. Geol. 12, 29–45.

Lister, G.S., 1982. A vorticity equation for lattice reorientation during plastic deformation. Tectonophysics 82, 351–366.

Lister, G.S., Dornsiepen, U.F., 1982. Fabric transitions in the Saxony granulite terrain. J. Struct. Geol. 4, 81–92.

Lister, G.S., Hobbs, B.E., 1980. The simulation of fabric development during plastic deformation and its application to quartzite: the influence of deformation history. J. Struct. Geol. 2, 355–370.

Lister, G.S., Williams, P.F., 1983. The partitioning of deformation in flowing rock masses. Tectonophysics 92, 1–33.

Lister, G.S., Paterson, M.S., Hobbs, B.E., 1978. The simulation of fabric development during plastic deformation and its application to quartzite: the model. Tectonophysics 45, 107–158.

Mancktelow, N., 1993. Computer program StereoPlotXL. ETH, Zürich.

Means, W.D., 1977. A deformation experiment in transmitted light. Earth Planet. Sci. Lett. 35, 169–179.
Means, W.D., 1989. Synkinematic microscopy of transparent polycrystals. J. Struct. Geol. 11, 163–174.
Means, W.D., Dong, H.G., 1982. Some unexpected effects of recrystallization on the microstructures of materials deformed at high temperature. Mitt. Geol. Inst. Eidg. Tech. Hochsch. Univ. Zurich 239a, 205–207.
Panozzo-Heilbronner, R., Pauli, C., 1993. Integrated spatial and orientation analysis of quartz c-axes by computer-aided microscopy. J. Struct. Geol. 15, 369–383.
Panozzo-Heilbronner, R., Pauli, C., 1994. Orientation and misorientation imaging: integration of microstructural and textural analysis. In: Bunge, H.J., Siegesmund, S., Skrotzki, W., Weber, K. (Eds.), Textures of Geological Materials. DGM Informationsgesellschaft Verlag, pp. 147–164.
Poirier, J.P., Guillope, M., 1979. Deformation induced recrystallization of minerals. Bull. Mineral. 102, 67–74.
Rasband, W., 1995. Computer Program Image 1.57. National Institute of Health. Research Services Branch, developed at the U.S. National Institutes of Health and available on Internet at http://rsb.info.nih.gov/nih-image.
Ree, J.H., 1991. An experimental steady-state foliation. J. Struct. Geol. 13, 1001–1011.
Sander, B., 1950. Einführung in die Gefügekunde der geologischen Körper, 2. Die Korngefüge. Springer Verlag, 409 pp.
Schmid, S.M., 1994. Textures of geological materials: computer model predictions versus empirical interpretations based on rock deformation experiments and field studies. In: Bunge, H.J., Siegesmund, S., Skrotzki, W., Weber, K. (Eds.), Textures of Geological Materials. DGM, Informationsgesellschaft Verlag, pp. 179–301.
Schmid, S.M., Casey, M., 1986. Complete fabric analysis of some commonly observed quartz c-axis patterns. In: Hobbs, B.E., Heard, H.C. (Eds.), Mineral and Rock Deformation: Laboratory Studies — The Patterson Volume. Am. Geophys. Union, Geophys. Monogr. 36, 161–199.
Schmid, S.M., Handy, M.R., 1991. Towards a genetic classification of fault rocks: geological usage and tectonophysical implications. In: Müller, D.W., McKenzie, J.A., Weissert, H. (Eds.), Controversies in Modern Geology. Academic Press, London, pp. 95–110.
Schmid, S.M., Panozzo, R., Bauer, S., 1987. Simple shear experiments on calcite rocks: rheology and microfabric. J. Struct. Geol. 9, 747–778.
Schmidt, W., 1927. Untersuchungen über die Regelung der Quarzgefüge kristalliner Schiefer. Fortschr. Mineral., Kristallogr. Petrogr. 11, 334–343.
Simpson, C., 1980. Oblique girdle orientation patterns of quartz C-axes from a shear zone in the basement core of the Maggia Nappe Ticino, Switzerland. J. Struct. Geol. 2, 243–247.
Simpson, C., Schmid, S.M., 1983. An evaluation of criteria to deduce the sense of movement in sheared rocks. Bull. Geol. Soc. Am. 94, 1281–1288.
Tungatt, P.D., Humphreys, F.J., 1981. An in situ optical investigation of the deformation behavior of sodium nitrate — an analogue of calcite. Tectonophysics 78, 661–676.
Wenk, H.-R., Christie, J.M., 1991. Comments on the interpretation of deformation textures in rocks. J. Struct. Geol. 13, 1091–1110.
Wenk, H.-R., Canova, G., Molinari, A., Kocks, U.F., 1989. Viscoplastic modelling of texture development in quartzite. J. Geophys. Res. 94, 17895–17906.
Zhang, S., Karato, S., 1995. Lattice preferred orientation of olivine aggregates deformed in simple shear. Nature 375, 774–777.

Publication information
Tectonophysics (ISSN 0040-1951). For 1997 volumes 265–278 are scheduled for publication. Subscription prices are available upon request from the publisher. Subscriptions are accepted on a prepaid basis only and are entered on a calendar year basis. Issues are sent by surface mail except to the following countries where air delivery via SAL is ensured: Argentina, Australia, Brazil, Canada, Hong Kong, India, Israel, Japan, Malaysia, Mexico, New Zealand, Pakistan, PR China, Singapore, South Africa, South Korea, Taiwan, Thailand, USA. For all other countries airmail rates are available upon request. Claims for missing issues must be made within six months of our publication (mailing) date. For orders, claims, product enquiries (no manuscript enquiries) please contact the Customer Support Department at the Regional Sales Office nearest to you:
New York, Elsevier Science, P.O. Box 945, New York, NY 10159-0945, USA. Tel: (+1) 212-633-3730, [Toll Free number for North American customers: 1-888-4ES-INFO (437-4636)], Fax: (+1) 212-633-3680, E-mail: usinfo-f@elsevier.com
Amsterdam, Elsevier Science, P.O. Box 211, 1000 AE Amsterdam, The Netherlands. Tel: (+31) 20-485-3757, Fax: (+31) 20-485-3432, E-mail: nlinfo-f@elsevier.nl
Tokyo, Elsevier Science, 9-15, Higashi-Azabu 1-chome, Minato-ku, Tokyo 106, Japan. Tel: (+81) 3-5561-5033, Fax: (+81) 3-5561-5047, E-mail: kyf04035@niftyserve.or.jp
Singapore, Elsevier Science, No. 1 Temasek Avenue, #17-01 Millenia Tower, Singapore 039192. Tel: (+65) 434-3727, Fax: (+65) 337-2230, E-mail: asiainfo@elsevier.com.sg

US mailing notice – *Tectonophysics* (ISSN 0040-1951) is published bi-weekly by Elsevier Science B.V. (Molenwerf 1, Postbus 211, 1000 AE Amsterdam). Annual subscription price in the USA US$ 2505 (US$ price valid in North, Central and South America only), including air speed delivery. Periodicals postage paid at Jamaica, NY 11431.
USA POSTMASTERS: Send address changes to *Tectonophysics*, Publications Expediting, Inc., 200 Meacham Avenue, Elmont, NY 11003.
Airfreight and mailing in the USA by Publications Expediting.

NOTE TO CONTRIBUTORS

A detailed Guide for Authors is available on request. Please pay attention to the following notes:

Language
The official language of the journal is English.

Preparation of the text
(a) The manuscript should preferably be prepared on a word processor and printed with double spacing and wide margins and include an abstract of not more than 500 words.
(b) Authors should use IUGS terminology. The use of S.I. units is also recommended.
(c) The title page should include the name(s) of the author(s), their affiliations, fax and e-mail numbers. In case of more than one author, please indicate to whom the correspondence should be addressed.

References
(a) References in the text consist of the surname of the author(s), followed by the year of publication in parentheses. All references cited in the text should be given in the reference list and vice versa.
(b) The reference list should be in alphabetical order.

Tables
Tables should be compiled on separate sheets and should be numbered according to their sequence in the text. Tables can also be sent as glossy prints to avoid errors in typesetting.

Illustrations
(a) Illustrations should be submitted in triplicate. Please note that upon submission of a manuscript *three sets* of all photographic material printed *sharply* on *glossy paper* or as *high-definition laser prints* must be provided to enable meaningful review. Photocopies and other low-quality prints will not be accepted for review.
(b) Colour figures can be accepted providing the reproduction costs are met by the author. Please consult the publisher for further information.

Page proofs
One set of page proofs will be sent to the corresponding author, to be checked for typesetting/editing. The author is not expected to make changes or corrections that constitute departures from the article in its accepted form. To avoid postal delay, authors are requested to return corrections to the desk-editor, Mr. Herman E. Engelen, by FAX (+31.20.4852459\) or e-mail (h.engelen@elsevier.nl), preferably within 3 days.

Reprints
Fifty reprints of each article published are supplied free of charge. Additional reprints can be ordered on a reprint order form, which will be sent to the corresponding author upon acceptance of the article.

Submission of manuscripts
Three copies should be submitted to: Editorial Office *Tectonophysics*, P.O. Box 1930, 1000 BX Amsterdam, The Netherlands.
Submission of an article is understood to imply that the article is original and unpublished and is not being considered for publication elsewhere.
Upon acceptance of an article by the journal, the author(s) will be asked to transfer the copyright of the article to the publisher. This transfer will ensure the widest possible dissemination of information under the U.S. Copyright Law.
The indication of a fax and e-mail number on submission of the manuscript could assist in speeding communications. The fax number for the Amsterdam office is +31-20-4852696.
Authors in Japan, please note: Upon request, Elsevier Science Japan will provide authors with a list of people who can check and improve the English of their paper (before submission). Please contact our Tokyo office: Elsevier Science Japan, 1-9-15 Higashi-Azabu, Minato-ku, Tokyo 106; Tel. (+81) 3 5561 5032; Fax (+81) 3 5561 5045.
THERE ARE NO PAGE CHARGES

Submission of electronic text
In order to publish the paper as quickly as possible after acceptance authors are encouraged to submit the final text also on a 3.5″ or 5.25″ diskette. Essential is that the name and version of the wordprocessing program, type of computer on which the text was prepared, and format of the text files are clearly indicated. Authors are requested to ensure that apart from any such small last-minute corrections, the disk version corresponds exactly to the hardcopy.
If available, electronic files of the figures should also be included on a separate floppy disk.